Norwegian University of
Science and Technology

Experts in Team

Gullfaks Village 2013

Subsea Wet Gas Compression for Increased Production from Gullfaks Satellites

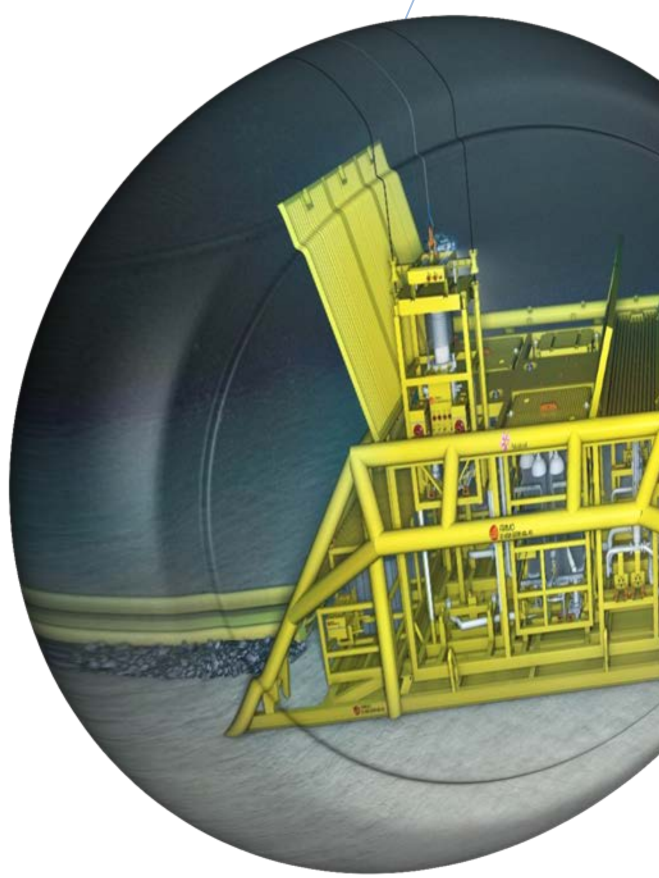

Group number 6:

Aysel Heydarova

Farad Kamyabi

Håvard Wilson

Joanna Pawlikowska

Mohamad Majzoub

Tarje Naterstad

Abstract

The objective of this report is to assess the influence of the installation of a subsea wet gas compressor in the field production and profitability for the Gullfaks South Satellite field, focusing on production from the L and M templates. Production problems due to liquid loading of the wells and flow assurance problems regarding hydrate formation were also considered.

The field behavior was simulated by simple dry gas equations programmed in Microsoft Excel and a gas-condensate reservoir material balance simulator, IPT-MATBAL. Three main cases were studied and compared to each other, natural depletion, natural depletion with reduction of separator pressure and installation of subsea wet gas compressor. The validity of the dry gas results was tested by comparing them to HYSYS simulations accounting for the condensate pressure loss. In order to assess the profitability of the studied cases, net present value calculations were performed based on the dry gas simulations and data given from Statoil.

Compared to natural flow, adding the subsea compressors improved the recovery from 57% to 75%, however the reduction in separator pressure yields a recovery rate up to 79%, which suggests that the best case scenario would be the implementation of a subsea compressor followed by a reduction in the separator pressure. Despite its lower recovery rate, the NPV calculations showed that the most profitable case was the installation of the compressor, this is because it produces larger amount of hydrocarbons earlier. Assuming dry gas for the simulation of the cases was found to be a good approach of the general field behavior, however there is a significant difference in the pressure loss, so the absolute values in this report should be used cautiously. Finally, calculations indicate that liquid loading might cause issues sometime during the production period of the field and that hydrate formation is not something to worry about unless there is shutdown of the production.

Table of Contents

List of Figures

List of Tables

Introduction

Driven primarily by the earth's population growth, the worldwide demand for energy is strongly increasing, and in the upcoming years it is expected to increase faster due to the rapid developments of highly populated countries such as China and India [1]. In 2012 more than 85% of the worldwide primary energy consumption was being provided by fossil fuels, from which only the natural gas accounts for 24% [2]; consequently, exploitation of natural gas as a primary energy resource is gaining importance every day.

In order to recover potential hydrocarbon reserves from mature fields with a declined reservoir pressure or young fields located far away from the processing facilities, boosting or compression (in gas fields) systems for installation on the seabed have been on the spotlight of the oil and gas industry. As usual, Statoil is leading the way for development of new technologies with two subsea compression projects, the first in the Åsgard field and the second for the Gullfaks South (satellite field), which is the core of this project.

Gullfaks is an offshore oil and gas field located 175 km. north-west of Bergen, Norway that started producing in December 1986. The Gullfaks satellites represent a large and profitable hydrocarbon province which has been developed in two phases, first an oil phase tied back to Gullfaks A platform and then a phase which primarily covers gas production tied to both Gullfaks A and C.

Among the Gullfaks satellites, this project is based on the production of Gullfaks South (a subsea development tied back to Gullfaks C platform) with focus on subsea production templates L and M, where Statoil (operator) and its partner Petoro have decided to invest in a subsea wet gas compressor for increasing the recovery of the field and maintain the plateau production to Gullfaks C for a few more years. Framo Engineering has been awarded the engineering, procurement and construction contract for the wet gas compression module.

The objective of this report is to assess the influence of the installation of a subsea wet gas compressor in the field production and profitability. The work will be presented with main focus on production figures and depletion of the reservoirs, supported by an economic analysis of the different scenarios. Some issues related to the production such as hydrate formation and liquid loading of the wells will be addressed by the end of this report.

Production Cases

- ## Plateau Production Approaches

In this section, three simple case studies of the production by natural flow for the Gullfaks South Satellite Field are conducted; the total satellite field required plateau rate is set to be 10x10^6 Sm^3/day. These cases have been studied with the objective of showing how the plateau of the field would be affected by different production approaches and which is the one that gives the longest production plateau. Table 1 shows the given data of the field.

Table 1. Given data for study of Gullfaks South

Gullfaks South L-M satellite system Pre-compression Phase (Start January 2009)	**East Tank L-Template Fault Block 13 Brent Formation**	**West Tank M-Template Fault Block 14 Brent Formation**	**Units**
G=GIIP-Gas cap (31 December 2008)	-	17,5E+9	Sm^3
Condensate from Gas Cap (31 December 2008)	-	4,4E+6	Sm^3
Oil legs: STOIIP (31 December 2008)	-	7,5E+6	Sm^3
Gas in Solution (from oil leg)	-	1,9E+9	Sm^3
Rs Solution Gas oil Ratio (oil leg) (31 December 2008)	-	248	Sm^3/Sm^3
rs Condensate gas ratio (gas cap) (31 December 2008)	-	251	Sm^3/MSm^3
STOIIP + Condensate (31 December 2008)	34,5E+6	-	Sm^3
GIIP + diss.gas (31 December 2008)	54,2E+9	-	Sm^3
Wells per template	4	3	-
Production days per year	328	330	days
Reservoir Temperature, T_R	128	112	°C
Pi, initial Res pressure (01 Jan 2009)	240	210	bara
Pi, initial Res pressure (1999)	459	446	bara
C, inflow Back pressure coefficient	1000	700	Sm^3/bar^{2n}
n, backpressure, exponent	0,8	0,8	-
Tubing MD	3515	2800	m
Tubing TVD	3100	2500	m
Ct, Tubing coefficient 7" (ID=6.094")	38152,4	41163	Sm^3/bar
Elevation coeff Tubing, S	0,43	0,34	-
C_{FL} 12".Template L-to-Towhead 66 m	1403054	-	Sm^3/bar
C_{FL} 8" Template-to-Towhead 62 m	466786	-	Sm^3/bar
C_{FL} 12".Template M-to-Towhead 64 m	-	1397663	Sm^3/bar
$C_{PL\ Pipeline}$ 14" Towhead-to-GFC 14000m (ID=0.32m)	148220	148220	Sm^3/bar
$C_{PL\ Pipeline}$ 8" Towhead-to-GFC 14000m (ID=0.197m)	32967	32967	Sm^3/bar
Separator pressure GFC (Inlet Sep)	60	60	bara
Top GFC riser pressure (High pressure mode)	65	65	bara
Top GFC riser pressure (Low pressure mode)	25	25	bara
Gas molecular weight (Methane)	19	19	kg/kmole
Gas specific gravity	0,66	0,66	-

A simplified field layout is shown in Figure 1. According to the operator of the field, one of the pipelines connecting the towhead with the platform, the 8" pipeline, is used for transportation of hydrocarbons from template N, which is not part of this study. However, further in this report, considerations for transporting produced hydrocarbons from templates L and M through this pipeline will be taken into account.

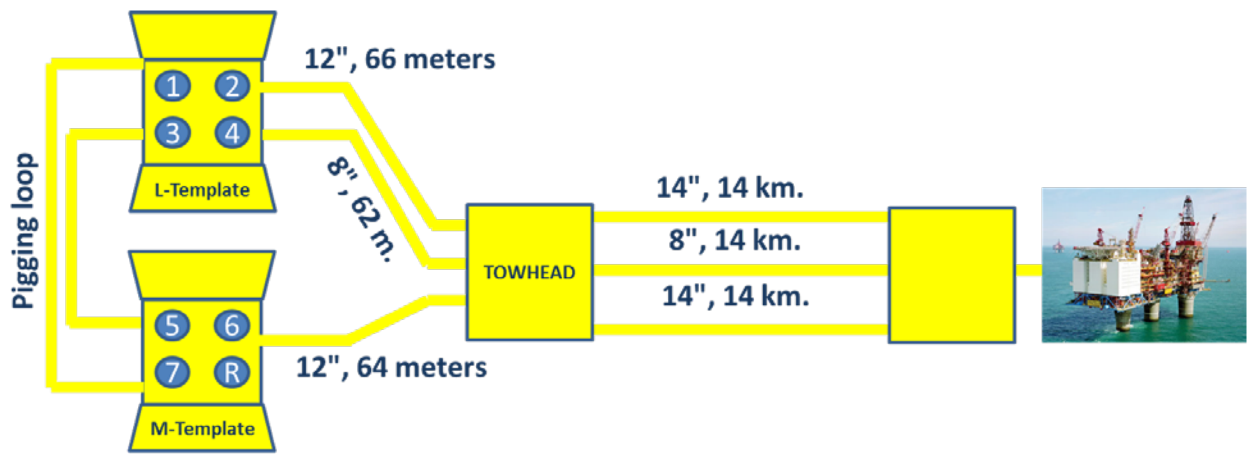

Figure 1. Simplified Gullfaks South layout

In order to develop a model of the field production using Microsoft Excel, the following assumptions and simplifications were taken:

- Dry gas and independent reservoirs for each template
- No aquifer effect
- No rock expansion
- Horizontal pipelines and flowlines (no elevation)
- The given reservoir data is from 2008 (31st of December), therefore the field development is modeled from that year
- All the wells for each template are identical
- The towhead is a junction point or a so-called manifold in which the entering flows are commingled and distributed proportionally among the outlet pipelines
- The field production is controlled by using the choke valve at the wellhead
- No heat transfer throughout the production system (Isothermal)
- Pressure drops calculated with dry gas model, no hydrocarbon or water condensation considered

For further details regarding the equations used for this studies refer to the Appendix.

- **Case A**

Case A covers a plateau length analysis for templates L and M producing continuously in a 60/40 proportion, which is the proportion given initially with the field data. Figure 2 shows the pressure depletion of template L; at a gas rate of 6 million Sm^3 per day, this field is able to produce until 2019.

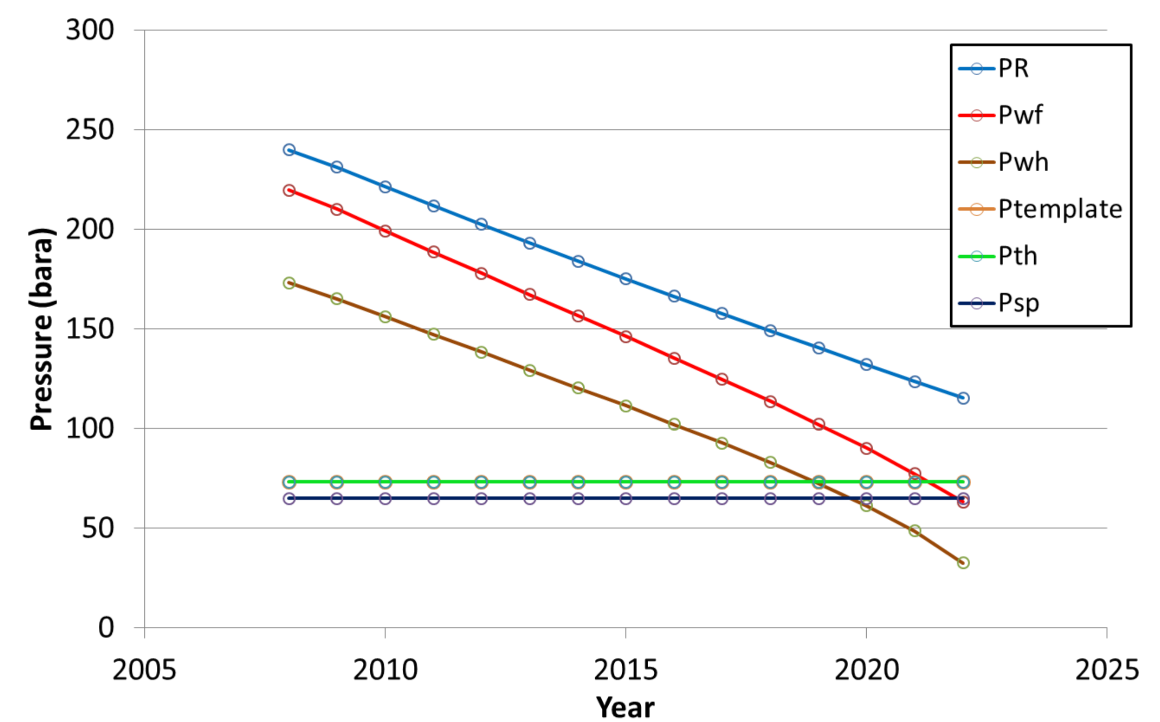

Figure 2. Pressure profile L-template, plateau production case A

Figure 3, on the other hand, shows the pressure profile of template M with time. When comparing the plateau production spans for both templates, it is possible to see that the total field plateau length will be determined by the shortest of them, which in this case is template M with plateau production ending in 2011. The fact that one of the templates reaches the end of plateau earlier means that the other template still has potential to produce when the plateau of the field has ended, this suggests that an adjustment in the flow rate of the templates will lead to an increased plateau length, which represents the cases B and C to be presented.

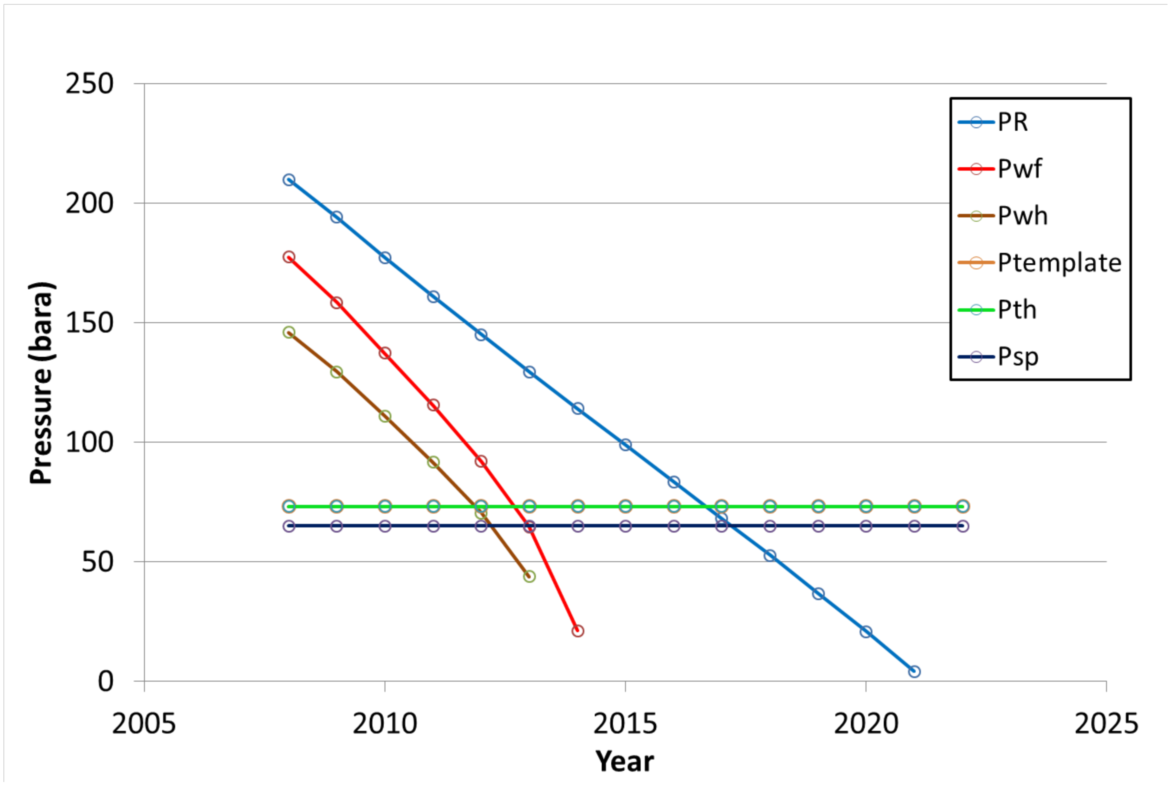

Figure 3. Pressure profile M-template, plateau production case A

- **Case B**

In this case, the production rates were fixed for finding a proportion such that both fields reached the end of natural production plateau simultaneously. This proportion was found to be 73/27 for templates L and M respectively. As for the first case, Figure 4 shows how the pressure drops during the time the field is in production for template L and Figure 5 shows the profile for template M.

The plateau length for the whole field (10 million Sm^3) was extended in contrast with case A by over four years, producing until September 2016. The only issue with this case is that the given production proportion (60/40) is not considered, which means that it might not be representing the real field production. Based on this, the following study (case 3) takes into account the given flow proportion until one of the reservoirs has reached the end of plateau.

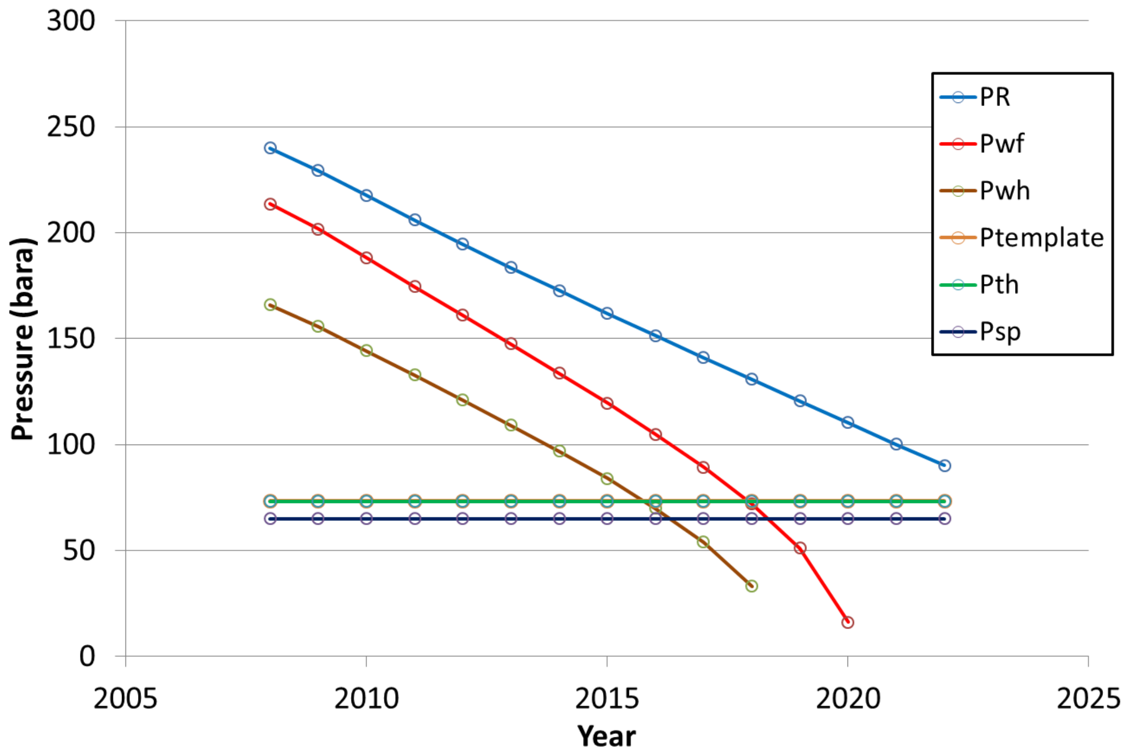

Figure 4. Pressure profile L-template, plateau production case B

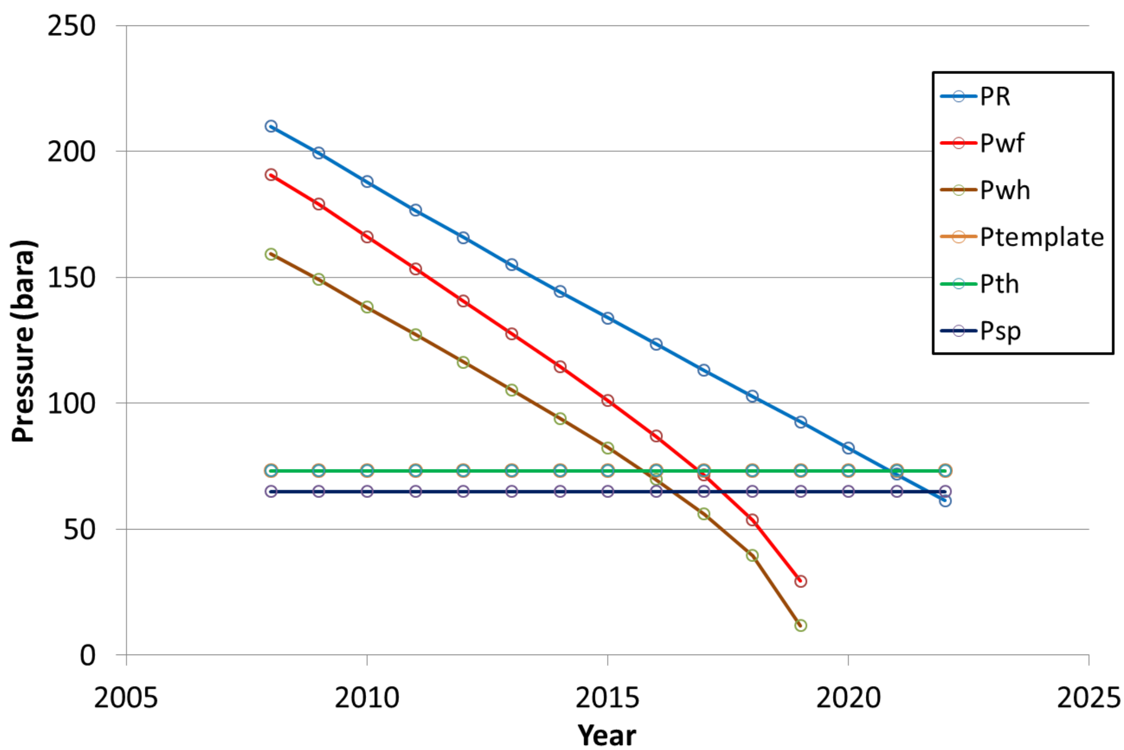

Figure 5. Pressure profile M-template, plateau production case B

o **Case C**

In this case, the production flows are set with the given value of 60/40 ratio for templates L and M until one of the templates, template M, has a fully open choke (end of plateau for this template); from this point the rate proportion is changed in order to reach a simultaneous end of plateau for both templates and prolong the plateau of the field. The proportion found is 77/23; which results in plateau production until August 2016. The pressure profile for each template is shown below in Figure 6 and Figure 7.

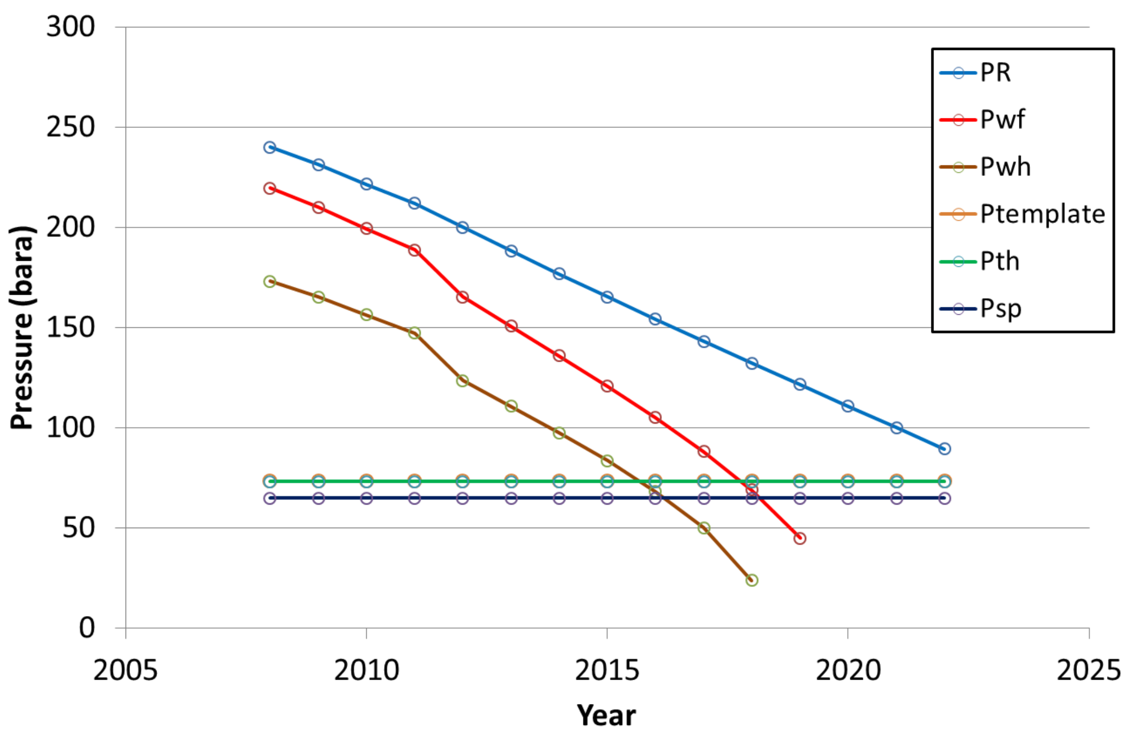

Figure 6. Pressure profile L-template, plateau production case C

It is important to notice from the pressure profiles for this case that there is a trend change in 2012 for two of the nodes (curves), the bottom hole pressure (Pwf) and the well head pressure (Pwh). This change is due to the variation in the flow rate, which for template L is increased whilst for template M is reduced. Based on the obtained results, this case is going to be used as the base case for further studies since it gives the longer plateau production time span considering the given flow rate proportion.

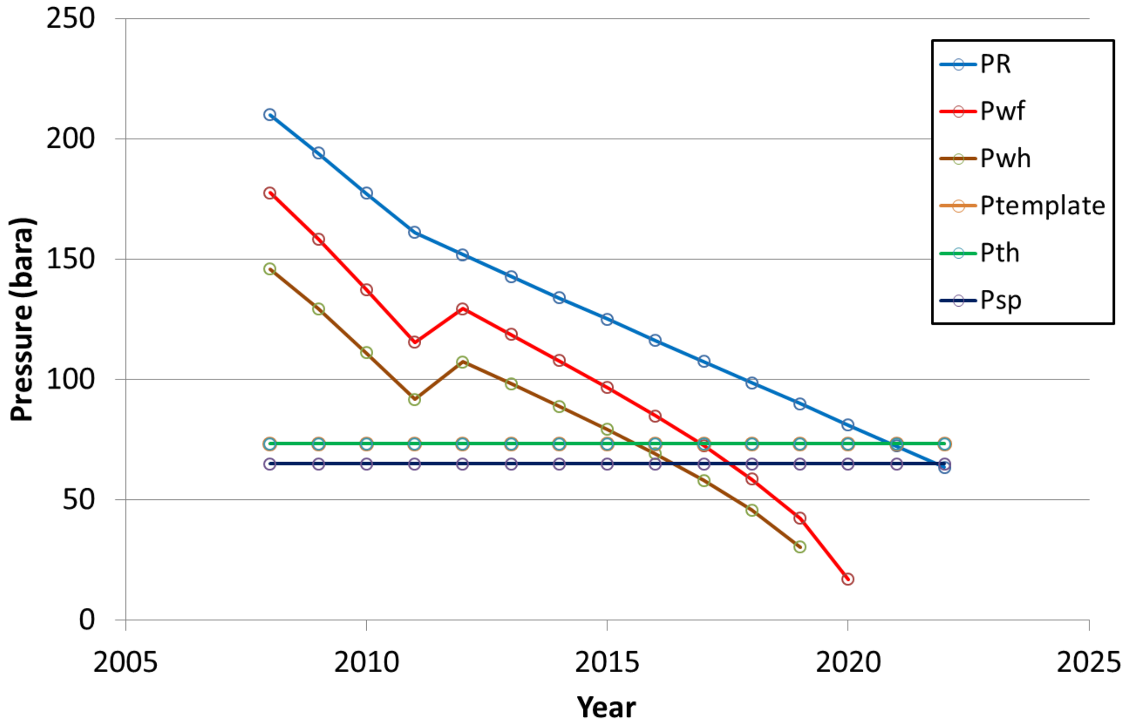

Figure 7. Pressure profile M-template, plateau production case C

- **Optimization of Well Configuration and Flow Distribution**

The recovery rate from a reservoir is strongly dependent on the distribution of the wells of the templates over the existing pipes. In this particular project, a study has been performed in order to find a production strategy that could lead to a better approach than the one studied for the previously presented cases, where the flow from both templates is commingled at the towhead and distributed evenly in the two 14" pipelines. The objective of this optimization is one basic parameter, the plateau length which is linked with larger amounts of gas produced in shorter periods.

Every well and pipe is given a number in order to make the assessment of the different cases simpler; see Figure 8 where the layout of the production templates L and M in Gullfaks South with the numbered wells and pipes is shown.

Besides the simplifications and assumptions stated before, several considerations had to be taken for the sake of convenience since a limited and less complex example is easier to follow and the interpretation becomes easier. The following assumptions were considered valid for this optimization study:

- No mixing of flow in towhead
- Pigging loop is used in the case of flowing some of the wells of one template through the pipeline of the other
- Only two pipes can be used for flow from towhead to the separators, the other pipeline has to be kept for production from template N

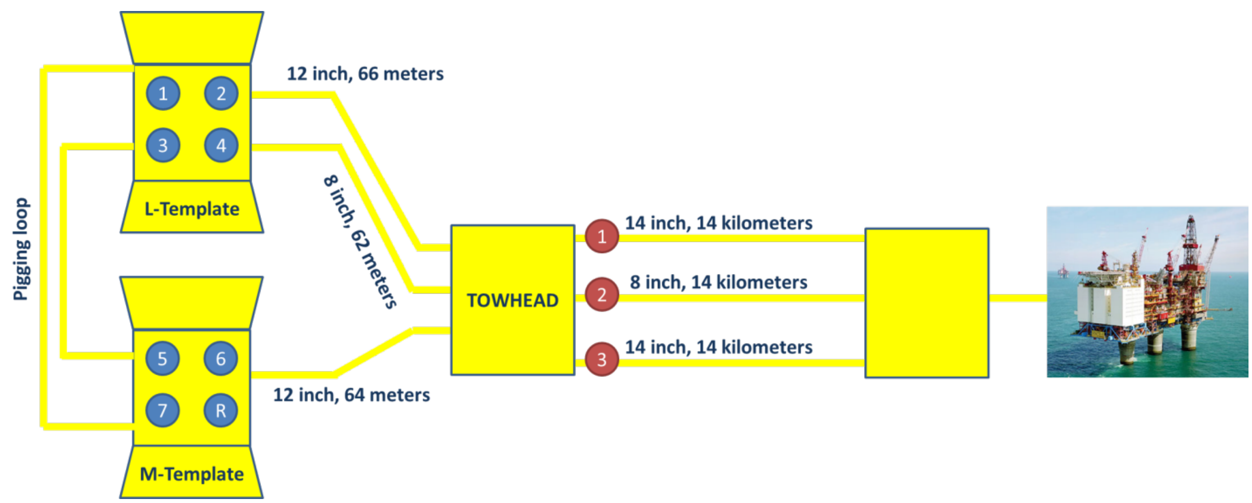

Figure 8. Simplified layout with numbered wells and pipes

All the calculations are based on the pressure difference of chokes between each wellhead available pressure and the template required pressure, ΔP_{choke}. As for case C from the previous section, starting with a 60/40 ratio of flow rates for template L and M respectively means that the rates should be adjusted at some point in order to reach a simultaneous end of plateau for both templates.

The critical node in this study, when compared to the previous case, is the towhead pressure (Pth) since there is no mixing, thus the towhead pressures are different for each pipe and for each case. For example, having the same flow rate a pipeline with a different diameter ends up with different towhead pressure. In a similar way, different number of the wells flowing through a pipe results in different flow rate in the pipe and evidently some other value for the towhead pressure.

In this study, the result of 229 combinatorial cases has been determined. Among these cases, only 18 were unique and the other ones were simple combinations of these cases derived from the assumption of identical wells. Table 2 shows the matrix of cases, where the red colored cases represent those in which the production of the field at the given proportion is unfeasible due to the large pressure drop in the pipeline.

Table 2. Matrix of cases for well distribution

Case	1	2	3	4	5	6	7	8	9	10	11	12	13	14	15	16	17	BC
Well	Flowing through pipeline																	
1	1	1	2	1	1	1	1	1	1	1	1	1	1	1	1	1	3	1/3
2	1	1	2	1	1	3	1	1	2	1	1	1	1	1	1	3	3	1/3
3	1	1	2	1	3	3	1	2	2	1	2	1	2	1	3	3	3	1/3
4	1	1	2	3	3	3	2	2	2	2	2	1	2	3	3	3	3	1/3
5	3	2	3	3	3	3	2	2	2	2	2	1	1	3	3	3	3	1/3
6	3	2	3	3	3	3	2	2	2	1	1	2	1	1	1	1	1	1/3
7	3	2	3	3	3	3	2	2	2	1	1	2	1	1	1	1	1	1/3

The following chart, Figure 9, shows the cumulative production of gas and length of plateau for each of the feasible cases. As mentioned before, these calculations have been done for the plateau period and therefore the figures for gas production and plateau length are proportional.

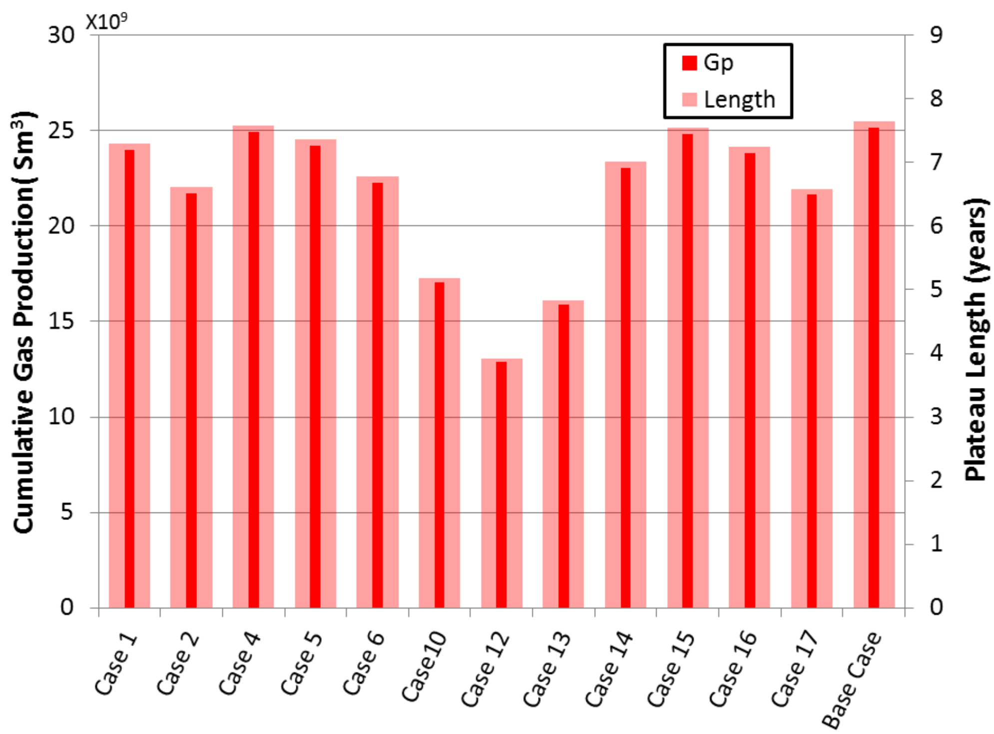

Figure 9. Plateau length for well distribution cases

After trying 229 cases, the case in which the flow is distributed 50-50 into two 14" pipes gave the longest natural flow time, this corresponds with case 3 (base case) from the previous section. It is also important to notice that this optimization approach was targeted to give a guess of the best well configuration and although no better configuration than the presented in the base case was found, the attempts tended to be at least fairly successful and led to the following claims:

- The 8" diameter pipeline cannot take flows larger or equal to 4 million Sm^3/day, otherwise the pressure balance on the choke will be negative from the first year (pressure required larger than available).
- When 2 or more wells from one template flow through the pipeline of the other template, the plateau length will be determined by the choke of these wells and vice versa.

- **Natural Flow Depletion**

This section covers the plateau production period presented previously in the base case (case C), with depletion of the field rate until the minimum economic value (2 million Sm^3/day) is reached. The idea is to study the entire life span of the field and not only the plateau period.

One of the key differences between this case and case C is the consideration of a gas-condensate reservoir in which the condensate will influence the pressure and the mobility of the fluids in the reservoir; this is done mainly to account for the liquid production since even small amounts of liquid might be highly profitable for the project. Pressure drops are still computed assuming dry gas. The gas-condensate reservoir material balance is solved by using IPT-MATBAL, an MBO PVT (modified black oil PVT) tool developed by Milan Stanko, a PhD. Student in the Department of Petroleum Engineering and Applied Geophysics, NTNU. For further details regarding the IPT-MATBAL solution refer to the Appendix of this report.

The production rate was reduced once the available pressure was no longer larger than the required for a fixed rate (negative choke pressure drop), and this was done in steps of 2 million Sm^3/day; meaning that four flow rate adjustments were required before reaching the field's minimum economic rate (2016, 2018, 2020 and 2023).

Based on what is shown in Figure 10 and Figure 11, the production of Gullfaks South would reach its economical limit in 2029. Notice that both figures have changing trends in the bottom hole pressure (Pwf) and the wellhead pressure (Pwh) due to the variation of the field in each of the templates (see Table 3).

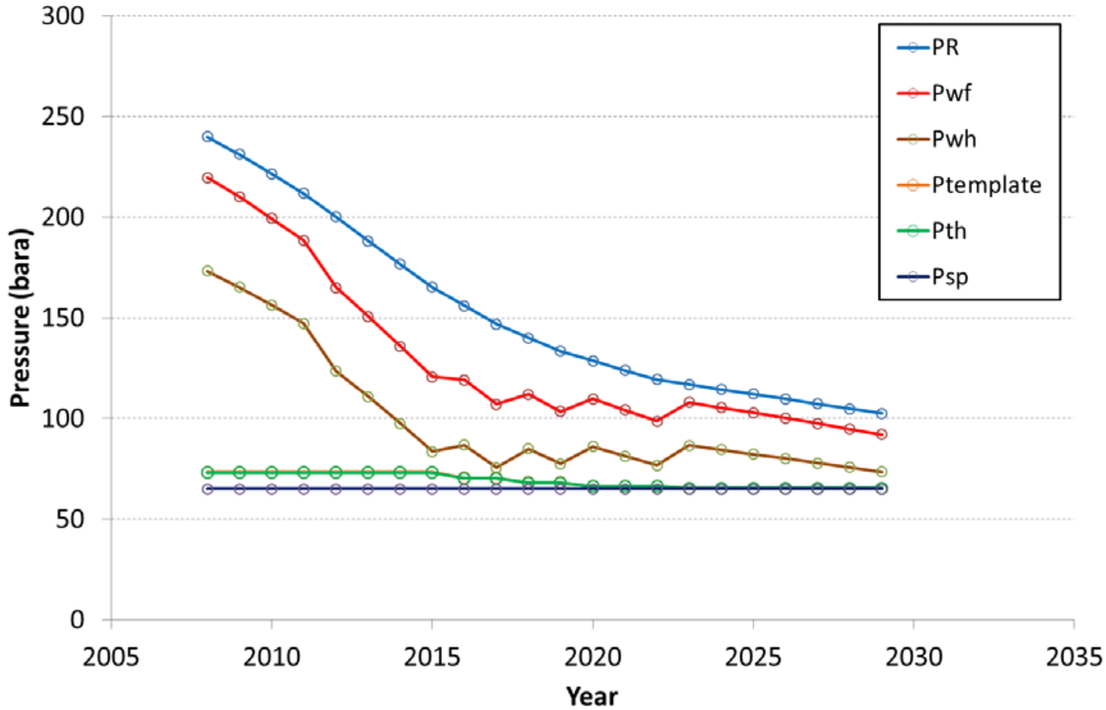

Figure 10. Pressure profile L-template, natural depletion

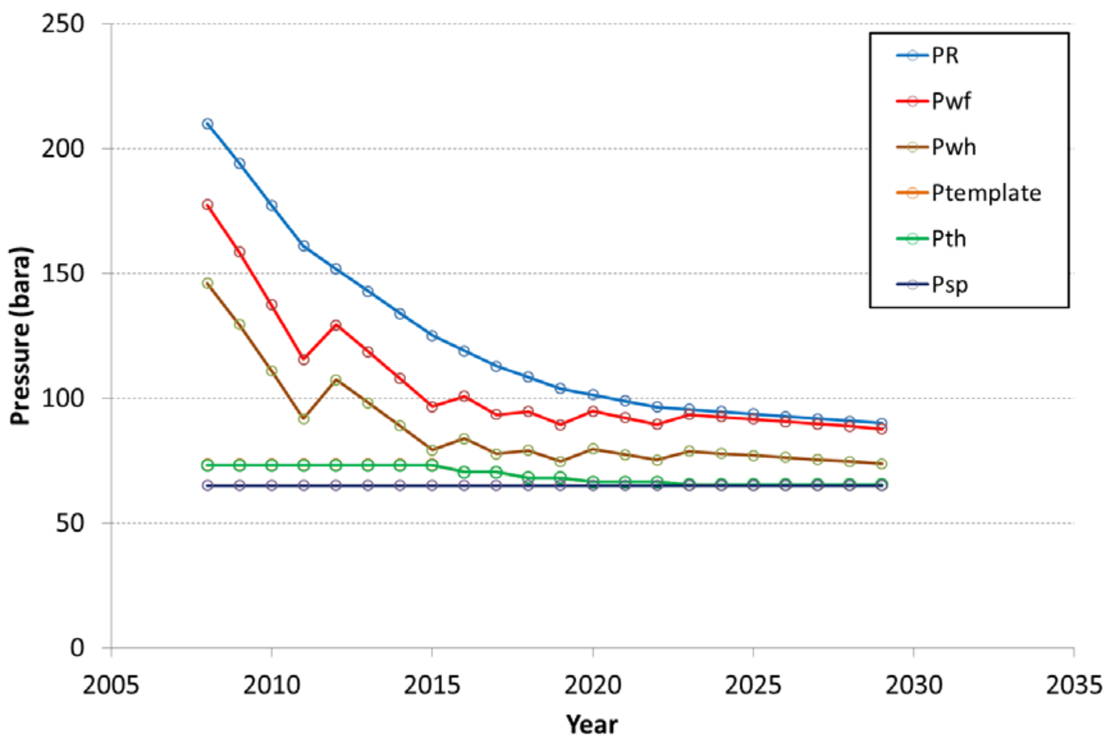

Figure 11. Pressure profile M-template, natural depletion

Table 3. Production flows from Gullfaks South, natural depletion

Year	2008-2011	2012-2015	2016-2017	2018-2019	2020-2022	2023-2029
L (Sm^3/day)	6,0E+6	7,7E+6	6,4E+6	4,8E+6	3,4E+6	1,8E+6
M (Sm^3/day)	4,0E+6	2,3E+6	1,6E+6	1,2E+6	650,0E+3	250,0E+3
Total (Sm^3/day)	10,0E+6	10,0E+6	8,0E+6	6,0E+6	4,0E+6	2,0E+6

The following chart, Figure 12, shows the field production of gas and condensate in standard cubic meters of oil equivalent. This gives an idea of the effect of the condensate in the field profitability. Based on this production profile, the total field is expected to have a 57% recovery factor with regards to the gas reserves.

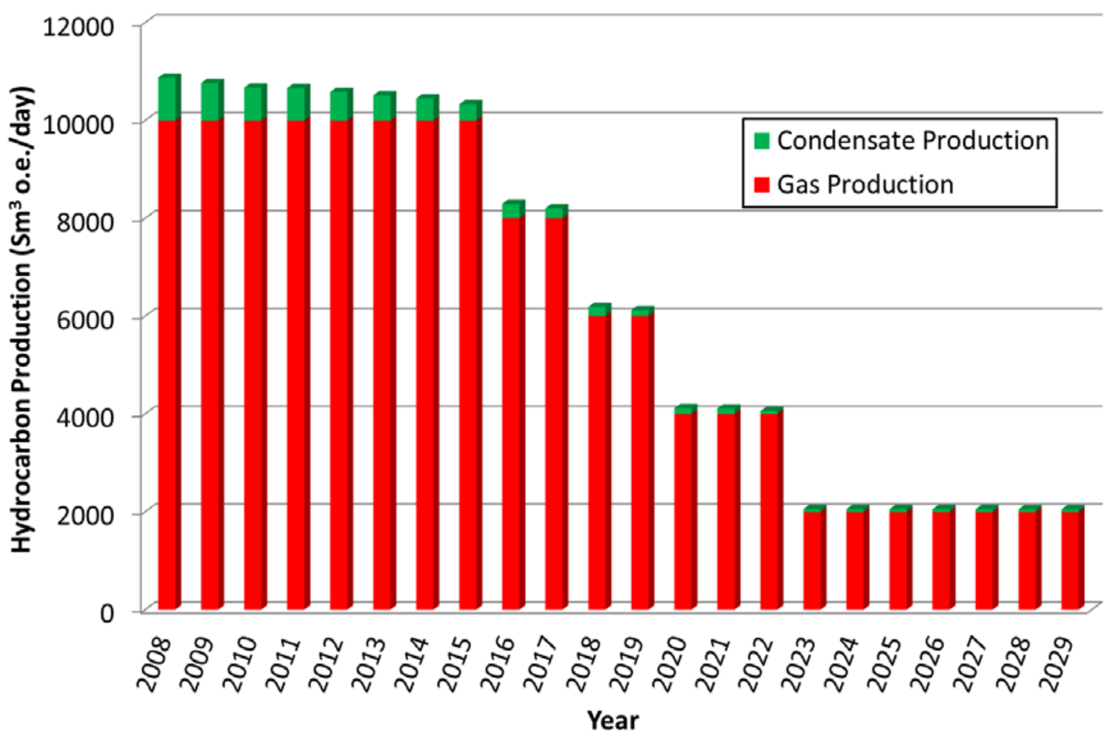

Figure 12. Production profile Gullfaks South in Sm^3 o.e/day, natural depletion

The amount of condensate produced is reduced due to the reduction in the solubility of oil in gas (rs) as the pressure of the reservoir depletes, this is shown in Figure 13 which was obtained from the IPT-MATBAL black oil property table.

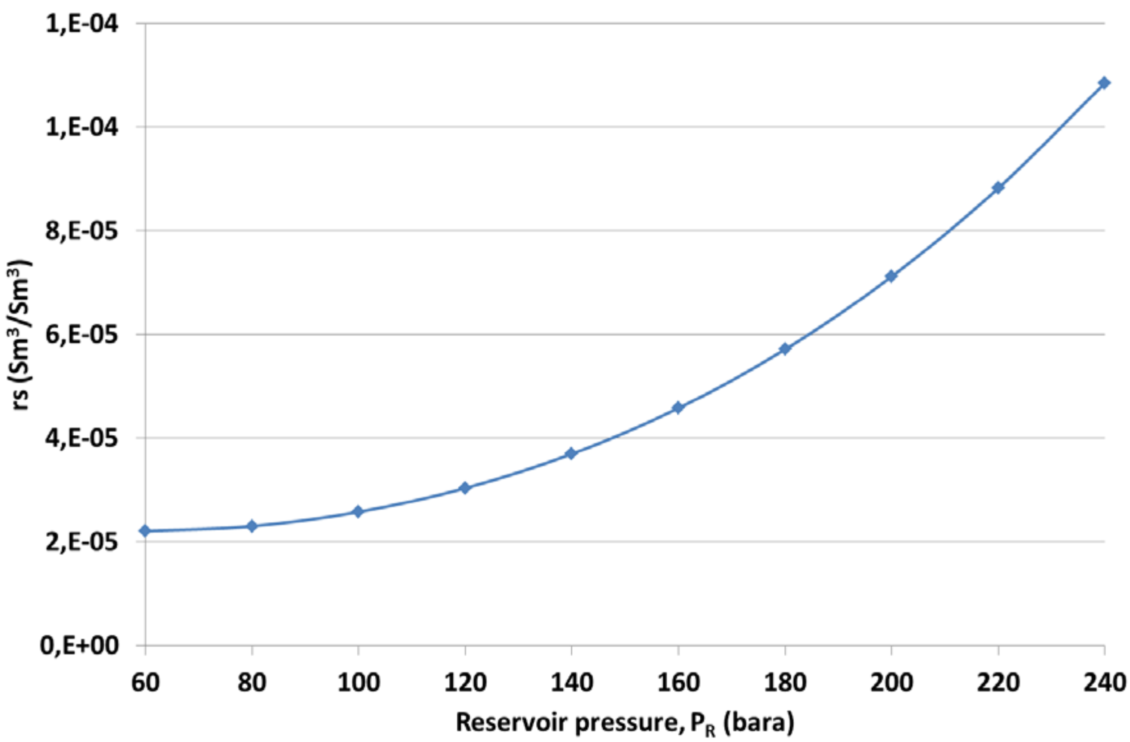

Figure 13. Solubility of oil in gas for template L, IPT-MATBAL

- **Subsea Compression**

In order to perform the study of the field production when the subsea wet gas compressor is installed it was necessary to obtain some information from the contract holder for the fabrication of this equipment, Framo Engineering. According to the manufacturer the system will use two 5-MegaWatt units that could be connected in series or in parallel operation mode, and each of the units has a maximum pressure boosting capacity of 32 bar.

The base case is also used as departing point in this study and once the end of plateau has been reached simultaneously for both fields (2016) a compressor is implemented at the towhead in order to extend for some years the production at plateau rate.

In this section, once the compressor is installed, the pressure equilibrium point (available and required pressure balance) will switch from the chokes to the compressor, with the peculiarity that the compressor will have a pressure lift whereas the chokes had a pressure drop. This means that with the compressor, the available pressure can be smaller than the required, since the compressor can lift this available pressure to reach the required one.

Based on the boosting capacity limitation of the compressor, two different compression stages were considered:

- Stage A: constant field production rate of 10 million Sm^3/day with increasing pressure lift across the compressor. End of stage when the pressure differential reaches 32 bar.
- Stage B: constant pressure increment of 32 bar with declining field production rate. Rate decline continues until the minimum field economical rate of 2 million Sm^3/day is reached.

Figure 14 clearly shows the two stages of operation of the compressor. As can be seen, the field will produce at plateau rate until 2018, which means that the plateau length has been extended for two years by means of the subsea compressor. Besides this, it is also important to notice that the field production has been extended for 4 more years, reaching the minimum economic field rate in 2033. As for the natural depletion case, Figure 15 shows the pressure profile for template L with the installation of the subsea compressor while Figure 16 shows the pressure profile for template M.

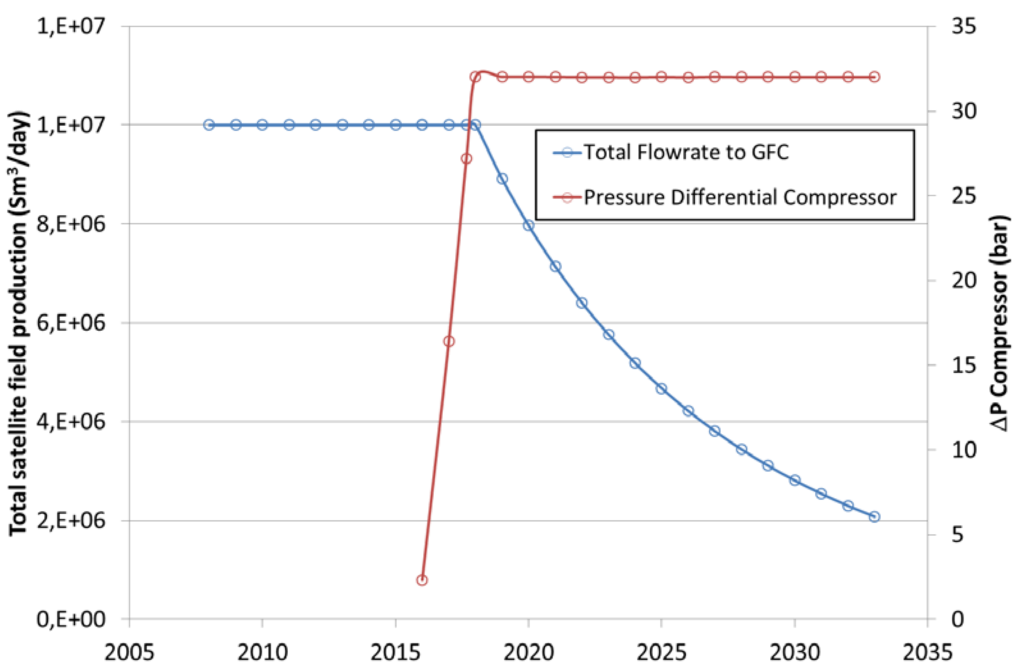

Figure 14. Field production and Compressor ΔP, subsea compression

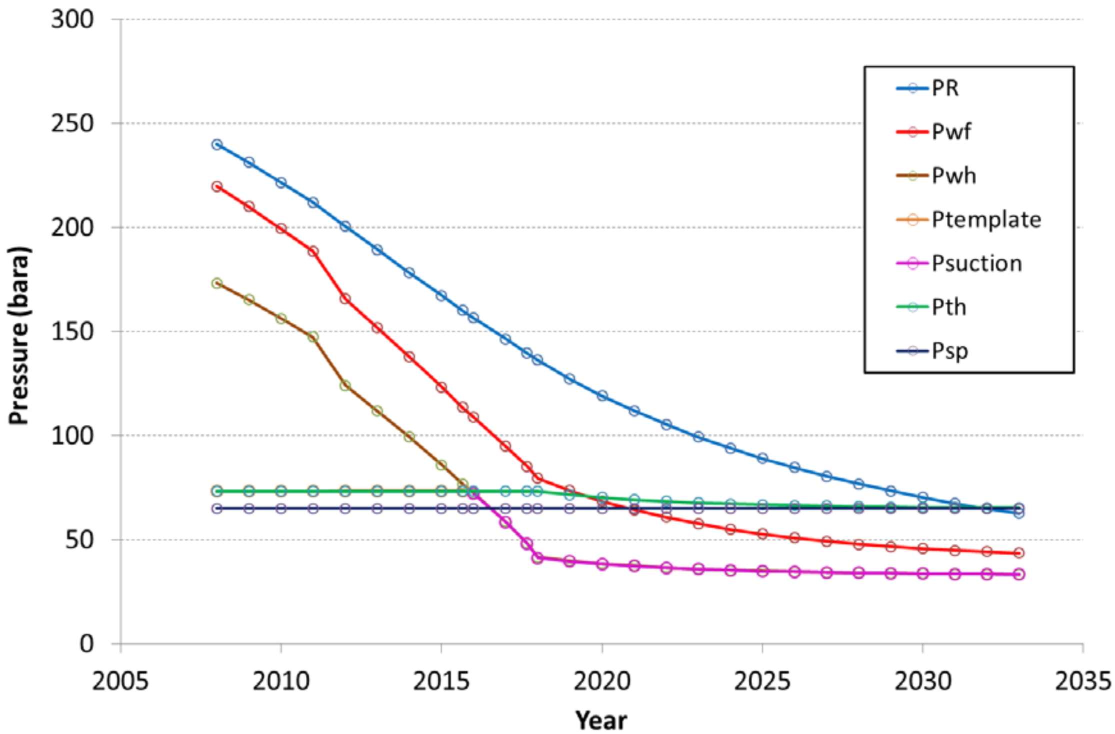

Figure 15. Pressure profile L-template, subsea compression

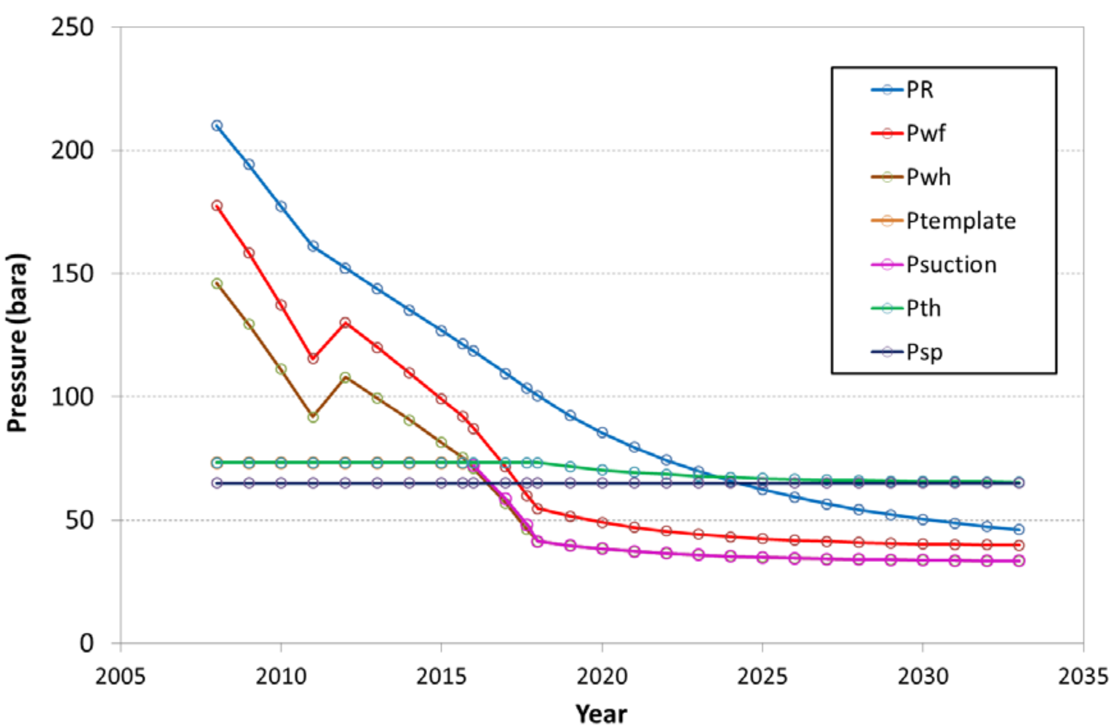

Figure 16. Pressure profile M-template, subsea compression

An important comparison between these figures and the ones shown in the natural depletion case is that the pressure curves of the nodes upstream the equilibrium point (choke in natural depletion and compressor in this section) cross with the ones downstream. This is due to the capability of the compressor to raise these pressures upstream to add up to the ones downstream.

As for the natural depletion case, Figure 17 shows the production profile of the field including condensates. With such production, the recovery of the field based on the gas reserves will be 75%. The explanation given before regarding the reduced amount of condensate produced with time is applicable to this case.

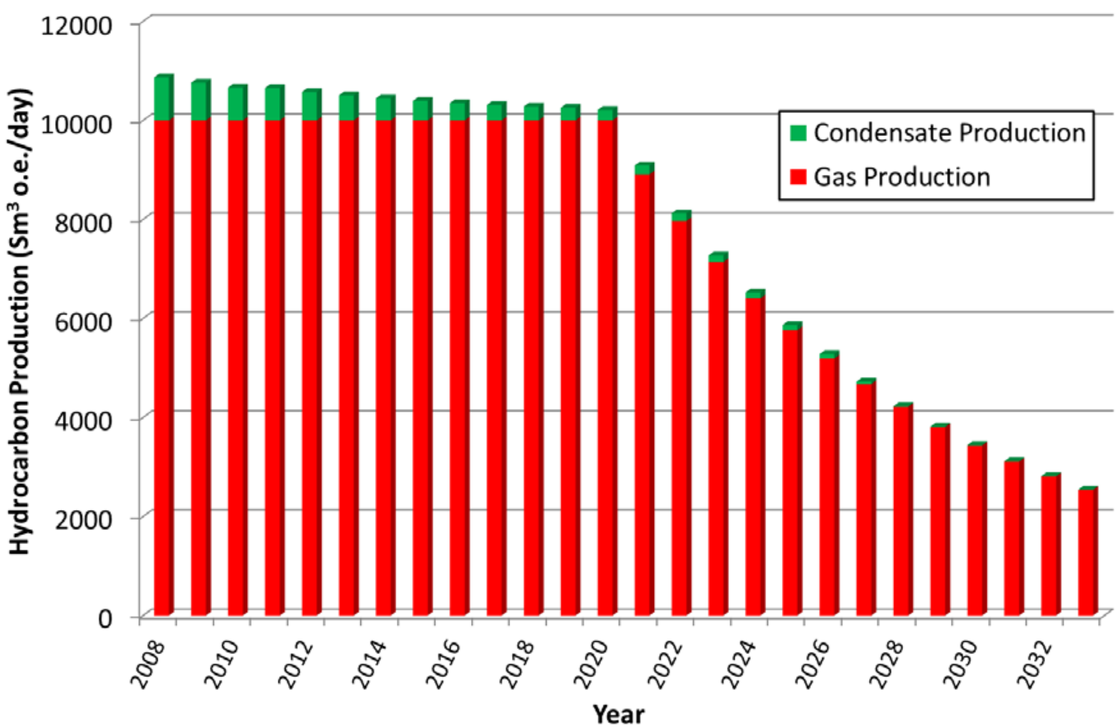

Figure 17. Production profile Gullfaks South in Sm^3 o.e/day, subsea compression

- **Reduction of Separator Pressure**

According to the field operator, there is a possibility to reduce the platform separator pressure in order to extend the economic life of the field. This was thought to be an important measure to be taken into account since it might define a parallel line of action with regards to the production of the field, which means that the reduction of the separator pressure could be chosen as an alternative to the installation of a subsea wet gas compressor, specially due to the uncertainties with regards to the lack of experience with the operation of such equipment subsea.

The pressure at the top of the riser (Psep) was set to be 65 bara for all the previously presented cases; for this particular study, once the field has reached the end of the 10 million Sm^3 plateau (case C) the separator pressure is reduced to 25 bar to prolong the plateau production period followed by a stage of natural flow depletion.

The pressure profile of template L is shown in Figure 18, where it is readily appreciable that in year 2016 there is a reduction of the separator pressure which makes the required pressure lower and therefore allows the production to be extended. The same can be seen in Figure 19 for template M. The trend change of the pressure profile in bottom hole (Pwf) and well head (Pwh) nodes is again due to the adjustment of the flow rates.

Figure 20 shows the production profile of the field when the separator pressure is reduced. It is important to notice that the field production has been extended for 10 years in comparison with the natural depletion case and 6 years when compared to the subsea compression case. Also, the recovery with the reduction of the separator pressure reaches 79%, which is the largest of the studied cases.

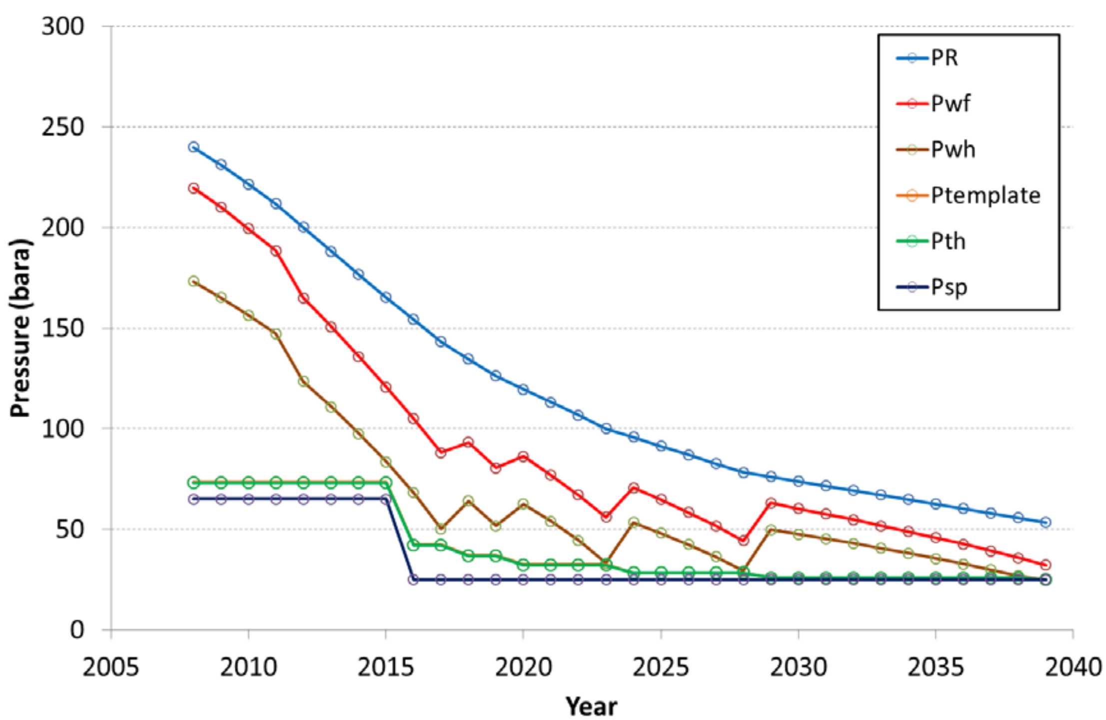

Figure 18. Pressure profile L-template, Psep reduction

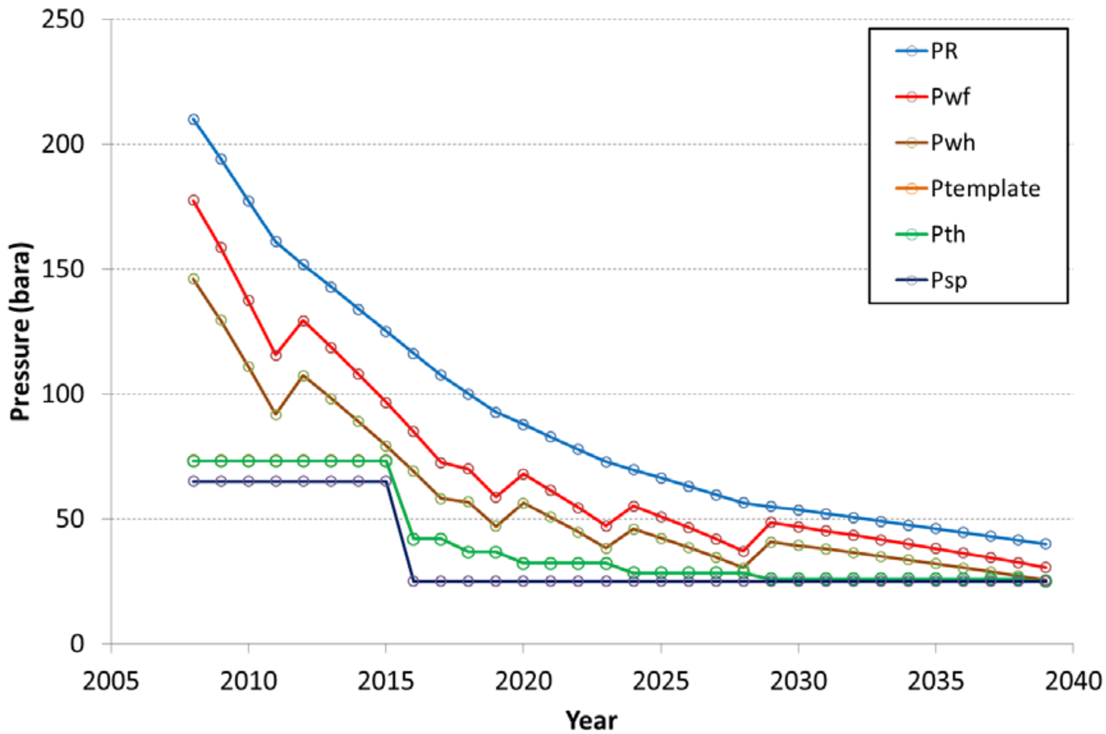

Figure 19. Pressure profile M-template, Psep reduction

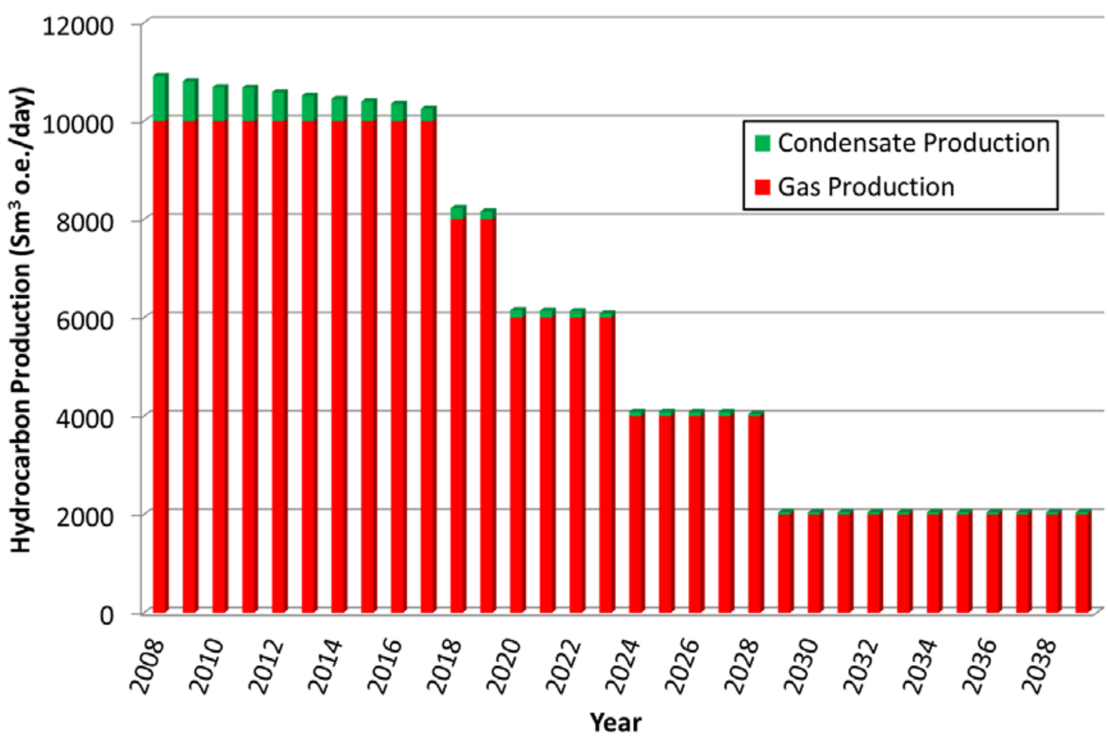

Figure 20. Production profile Gullfaks South in Sm[3] o.e/day, Psep reduction

This last case has yielded very promising results, and based on this, the implementation of such reduction in the separator pressure seems to be an advantageous alternative for the project. Nevertheless, the installation of a subsea wet gas compressor is actually beyond the production figures and recovery factors since it represents a state of the art technology that needs to be tested for future developments. The success in the installation of the subsea wet gas compressor for the Gullfaks South field has to be seen as a global success for the industry since it represents a new era for the subsea.

Additionally, the reduction of the separator pressure could be implemented jointly with the installation of the subsea wet gas compression system. This would represent the best case scenario in which the technology is implemented and the field is exploited to its limits. The study of such scenario has not been taken into account in this project due to lack of time, and since for the purpose of this work it is fairly simple to understand the effect that such joint implementation would have in the field production just by observing the results from the three main cases (natural depletion, subsea compression and reduction of separator pressure).

Compressor Performance

Each compressor has a different behavior when operating, which depends on the design and purpose of it; thereby, for a given flow rate (volumetric) and speed of the rotor, each compressor has a different pressure boost capacity. These variables are related in a graphical manner in what are so-called compressor performance curves or compressor maps. For the subsea compression case, no compressor performance has been taken into account, which means that the compressor capabilities (besides the 32 bar pressure boost) are not considered.

When trying to fit the values obtained previously in the subsea compression case with the provided compressor maps, it was necessary to do some adjustments. The main uncertainties were in the conditions of the compressor mapping test, basically because the given compressor map did not reach 5 Megawatts (reported compressor capacity). According to a compressor specialist at NTNU, Jesus De Andrade, the compressor map test conditions had to be changed, specifically the pressure was modified from the given value of 37,3 bar to 62,3 bar; and the temperature was slightly decreased from 62,3 °C to 60 °C. Indeed, these modifications brought the compressor map up to the desired 5 Megawatts as shown in Figure 21.

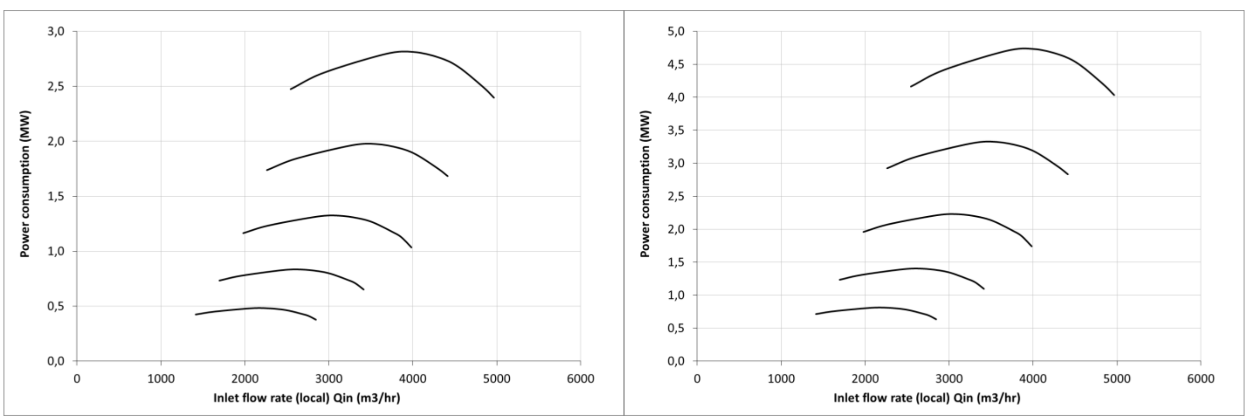

Figure 21. Compressor map for initial test conditions (left) and modified (right)

With the map obtained using corrected test conditions, still some adjustments needed to be done in order to fit all the operational points inside the compressor curves, specially the first operational point in which the pressure differential was too low (see Table 4). For this point, the discharge pressure was increased from 73,2 to 85 bara, assuming that it was possible to choke the discharge flow to the required pressure.

Table 4. Compressor operational points

Year	q	Psuc	Pdisc	dP	Operation Mode
-	sm^3/day	bara	bara	bar	-
2016	10,00E+6	68,5	73,2	4,8	Parallel
2017	10,00E+6	53,4	73,2	19,9	Parallel
2018	10,00E+6	41,3	73,2	31,9	Parallel
2019	8,91E+6	39,0	71,1	32,0	Parallel
2020	7,97E+6	37,9	69,9	32,0	Parallel
2021	7,14E+6	36,9	68,9	32,0	Parallel
2022	6,41E+6	36,1	68,1	32,0	Series
2023	5,76E+6	35,5	67,5	32,0	Series
2024	5,19E+6	35,2	67,3	32,0	Series
2025	4,68E+6	35,0	67,0	32,0	Series
2026	4,22E+6	34,6	66,5	32,0	Series
2027	3,81E+6	34,2	66,3	32,0	Series
2028	3,44E+6	34,0	66,0	32,0	Series
2029	3,11E+6	33,8	65,8	32,0	Series
2030	2,81E+6	33,7	65,7	32,0	Series
2031	2,54E+6	33,6	65,6	32,0	Series
2032	2,30E+6	33,5	65,5	32,0	Series
2033	2,01E+6	33,4	65,4	32,0	Series

Additionally, the operation of the compressor has to be changed in 2022 from parallel to series since the flow rate becomes too low and the operational point drifts outside the actual compressor map; only one example of this is shown in Figure 22 for the parallel operation and in Figure 23 for the series operation in year 2027. The rest of the compressor maps can be found in the Appendix with their respective operational points. Notice in the figure that the dashed lines represent the actual compressor map which is corrected by using the actual conditions of the inlet stream since the original map was gotten under the test conditions, which are different.

A compressor map is not only the power consumption curves, there are two more curves in which the ratio of the inlet and the outlet pressures (pressure ratio) and the polytropic efficiency are related to the volumetric flow rate and the velocity of the rotor, these curves are not presented on this report because they have no influence in the analysis and represent a large amount of pages.

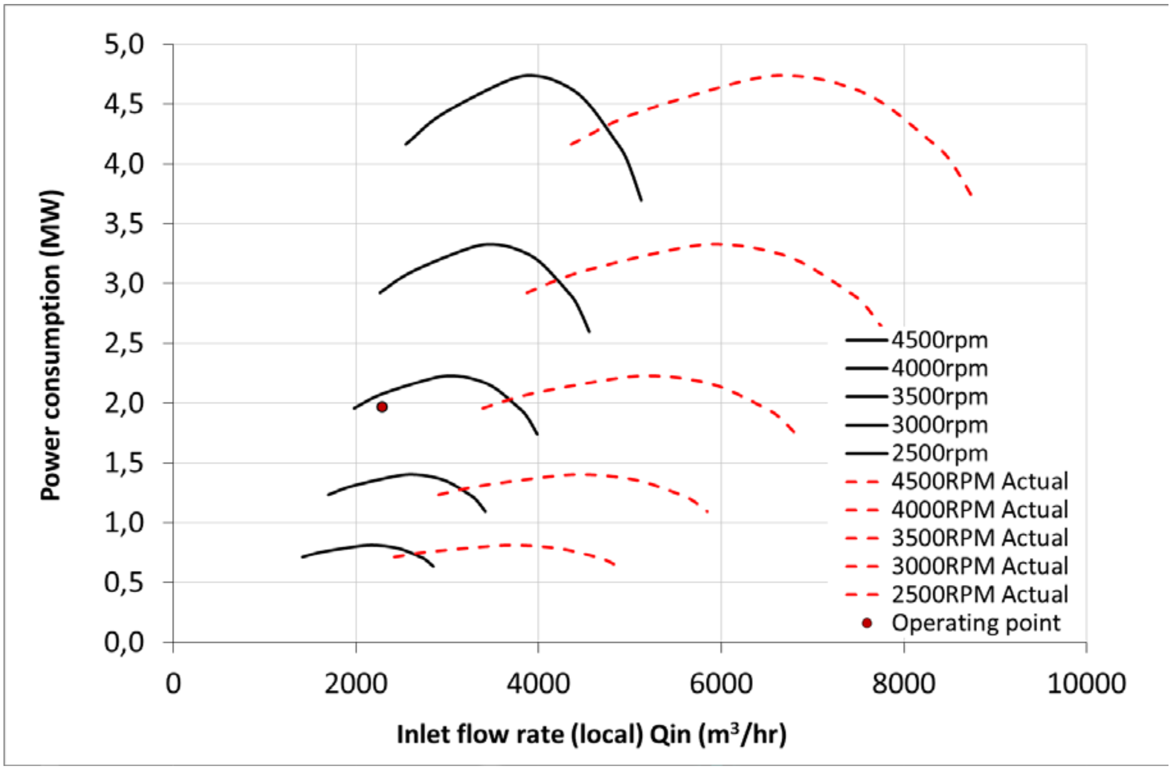

Figure 22. Compressor map, power, year 2027, parallel

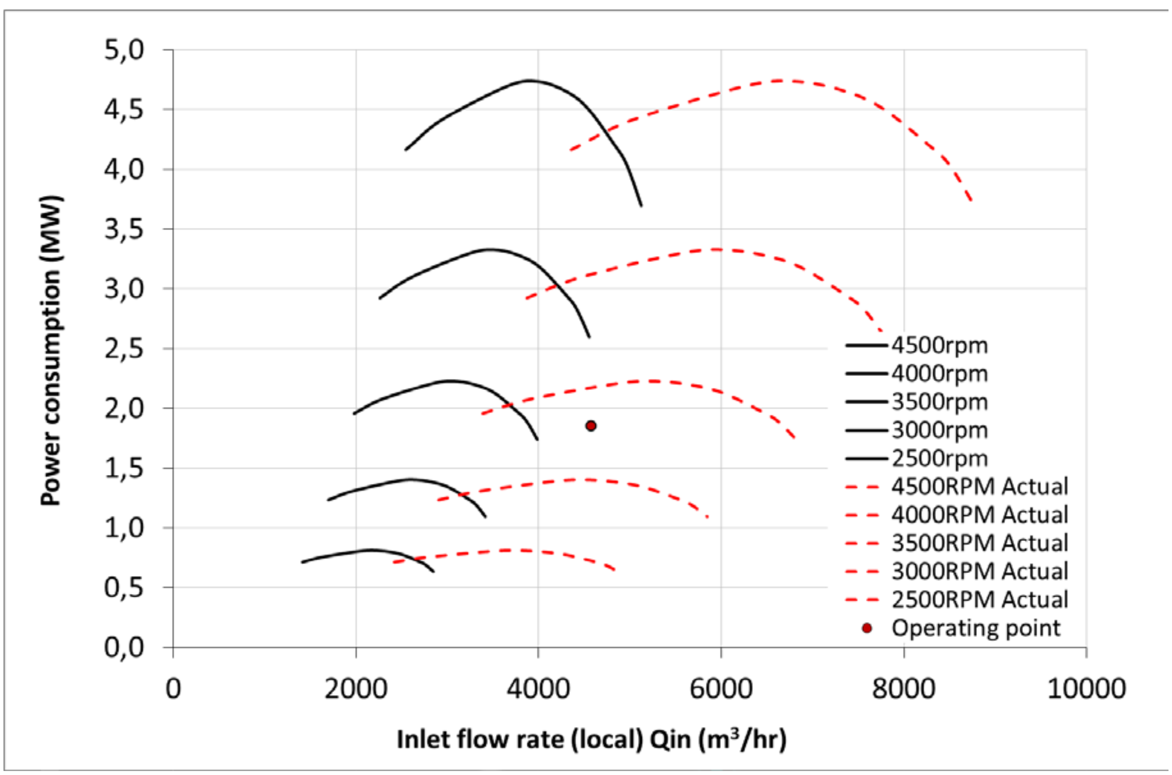

Figure 23. Compressor map, power, year 2027, series

Economic Analysis

In order to determine which of the aforementioned cases is likely to generate the greatest profits, an economic analysis should be performed. The best way of estimating the profitability of a venture in terms of present value, is to calculate the Net Present Value (NPV) and sensitivities, since analyzing the sensitivity of a venture provides information about the exposure of a venture to uncertainties, and what kind of unforeseen events may have the greatest impact on the end result.

In this report, the three studied cases will be considered and compared to one another: natural depletion, reduction of separator pressure and subsea compression, henceforth referred to as Case 1, Case 2 and Case 3, namely. Calculating the NPVs for these three main cases makes it easy to compare the results directly. A sensitivity analysis will be performed for the case that is deemed as most profitable.

In lieu of additional information, constant values for oil & gas ($100/bbl oil – 2,3 NOK / Sm^3 gas), exchange rate $ vs NOK (6NOK/$), inflation rate (2,5%) and cost of capital or discount factor (8%) are used in determining the NPV of the respective cases. Taxation rate is fixed at 78%, all capital expenditures are written off (depreciation) linearly over the next six years following investment.

For the first two cases, drilling expenditures (assuming no well stimulation / intervention will be required, all wells have been drilled), operations expenditures and capital expenditures have not been provided. As these expenses are directly related to the window of production, which will vary considerably from case to case, this is likely to skew the results of this analysis somewhat.

For Case 2, it has been estimated by Statoil that the reduction of the separator pressure at the platform will yield an additional cost of 1,0 Billion NOK. This consideration has been implemented in the NPV calculations.

For Case 3, capital expenditure estimates have been found regarding the EPC of the compression module (Framo Engineering), the required platform operations (Apply Sørco) and the subsea modifications (Subsea 7). Additionally, operational expenditures (energy, CO_2 & NOx tax) have been provided by Statoil for a given time window (until 2029); however, as the calculation presented earlier in this report shows, this window can be prolonged significantly. Therefore, to account for OPEX in the later years, OPEX has been calculated by using cost of electrical power and the compressor power consumption, with an additional cost of 20% to account for losses + additional costs (CO_2 & NOx tax, namely).

Figure 24 shows the cumulative NPV estimated for each of the cases, notice that there is difference in trend after year 8 when the modifications are implemented, the subsea wet gas compressor is installed for Case 3 and the separator pressure is reduced for Case 2.

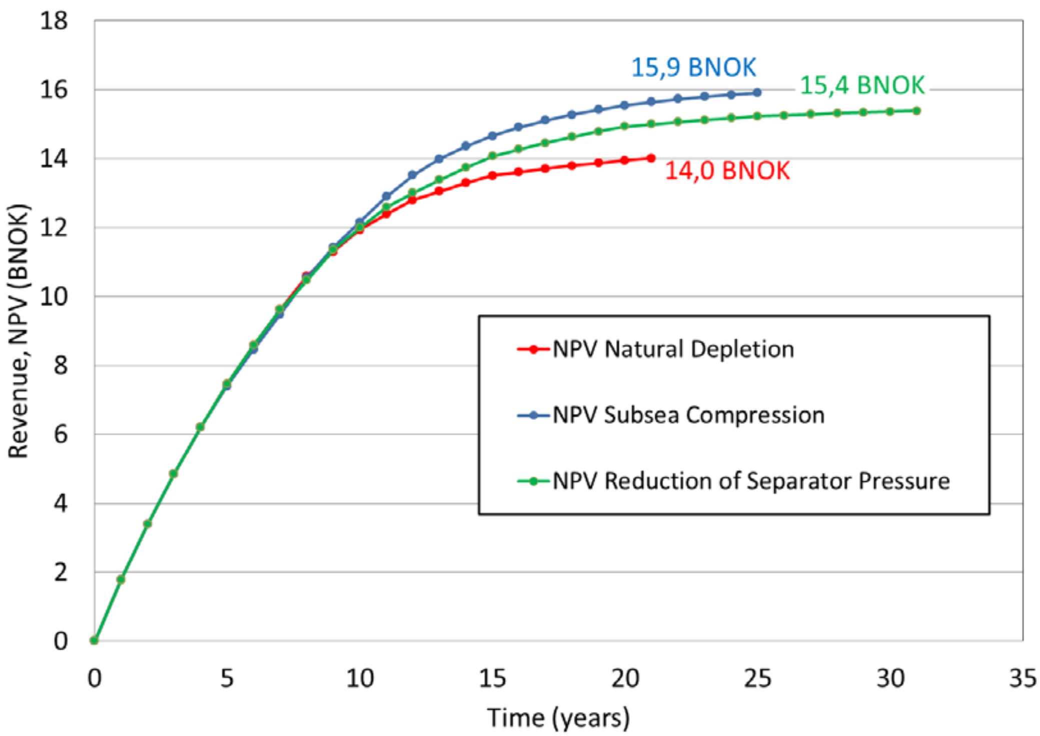

Figure 24. Estimated cumulative NPV, three cases

It is observed that the difference between Case 2 and Case 3 is relatively minor, but the crucial difference lies in that time of recovery is significantly shorter if producing with a compressor. This is crucial for the financial benefit of a company since current holdings can be reinvested into new ventures, meaning that today's income is a lot more worth than tomorrow's income, even if tomorrow's discounted income equals today's income in NPV.

A closer look to the differences between each of the cases gives a clear idea of what are the factors affecting the final cumulative NPV of each of them. Figure 25 shows the yearly cumulative NPV difference between the subsea compression case and the natural depletion; whereas Figure 26 presents the difference between the subsea compression case and the separator pressure reduction case.

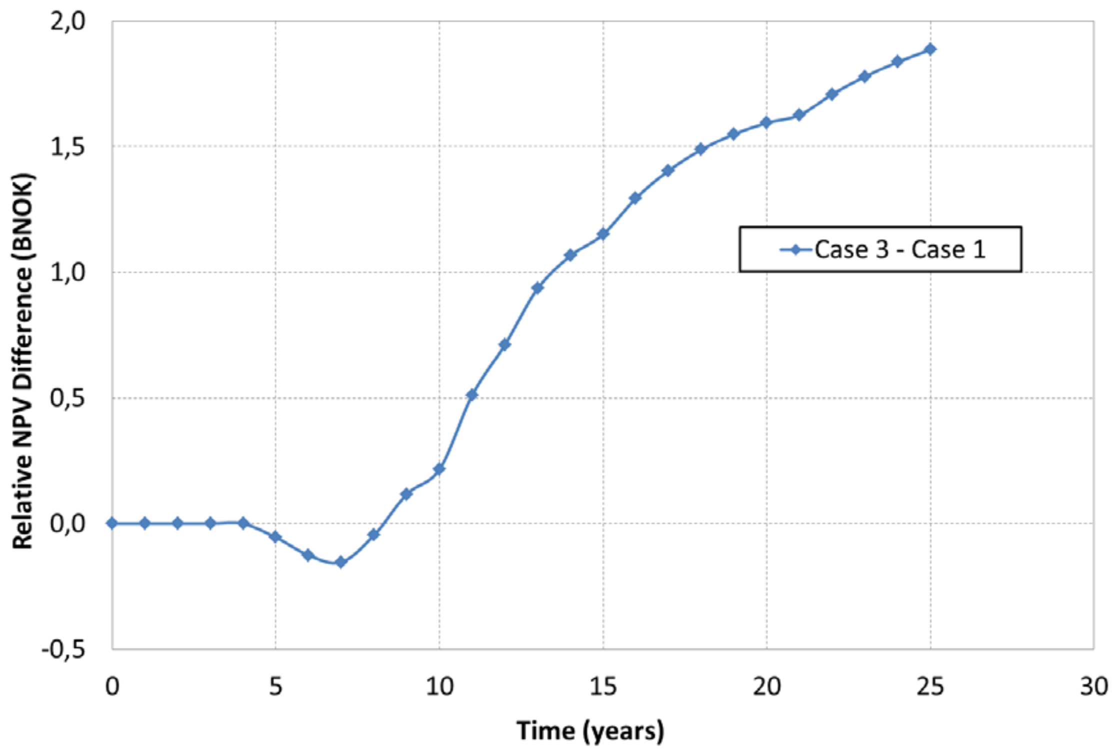

Figure 25. NPV difference, Case 3 minus Case 1

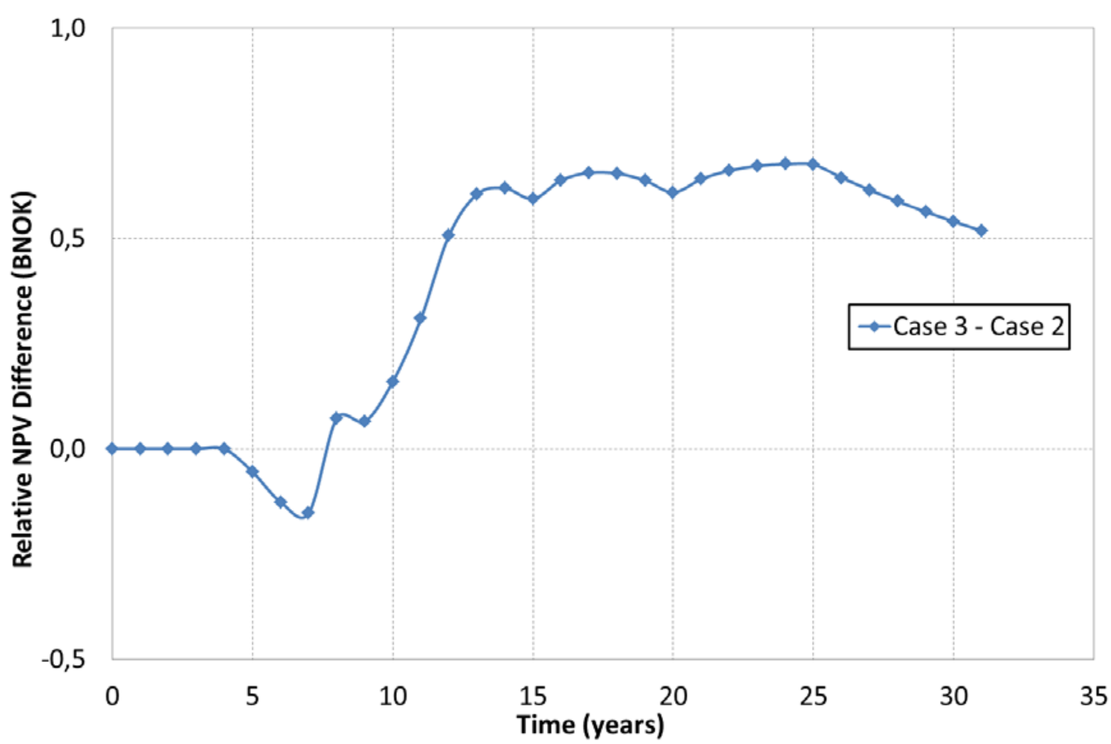

Figure 26. NPV difference, Case 3 minus Case 2

Based on the presented results in Figure 25, the additional costs of installing the compression module cause Case 1 to yield greater profits the first 8 years, after which there is no doubt that Case 3 is the most profitable one. In the comparison described in Figure 26, the relative difference is significantly less than for Figure 25. It bears mentioning, however, that Case 3 still surpasses Case 2 in profitability before end of production mainly because the length of the plateau is longer and therefore more revenues are acquired earlier. Adding to that the fact that reducing the separator pressure while producing with a compressor is still a viable option; the arguments presented thus far indicate that producing the satellite field using a subsea compressor assembly is the most profitable alternative.

- **Sensitivity Analysis**

Since Case 3 has been deemed the most promising, this will be the basis of the sensitivity analysis. It has been determined that the project is likely to be most sensitive to oil & gas prices, cost of capital rate, capital cost and downtime (due to maintenance, accidents, etc.), and as such, these will be the focus of the sensitivity analysis.

In order to weigh the sensitivity of the NPV calculations to the previously mentioned parameters, a simple, readily understandable tool has been used. This tool is widely known as a spider diagram, a representation in which the variation in a variable is plotted versus the relative variation (in percentage) of several key parameters.

As can be observed in Figure 27, even a significant increase in cost yields a minor impact on the profitability of the project, compared to fluctuations in cost of capital, oil price and downtime. By producing the field at all, Statoil is already exposed to fluctuations in cost of capital and oil price, and therefore it can be assumed that the added impact these considerations have with regards to profitability, comparing Case 1 and Case 2 to Case 3, is negligible.

As it stands, the compressor assembly is unqualified, and as such, reliability can prove to become an issue, causing downtime (maintenance, waiting for specialists to arrive at the scene, waiting for equipment to replace broken modules, etc.), and since the compressors are situated on the seafloor, it can be expected that repairs will be time consuming. Figure 28 shows a detailed sensitivity analysis of the downtime during compressor operation; this figure clearly shows that even a 5% increase in annual downtime represents significant loss of revenue and therefore the reliability of the equipment is one of the main factors that should be taken into account when deciding for projects of this magnitude.

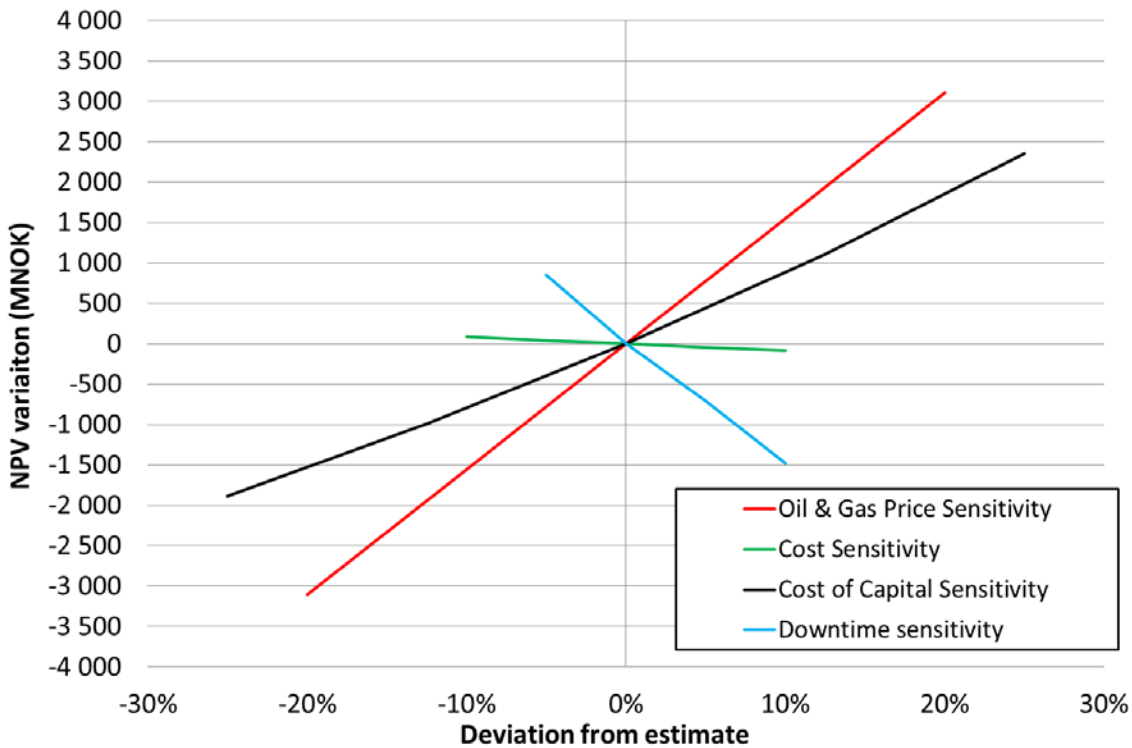

Figure 27. Spider diagram for cumulative NPV sensitivity

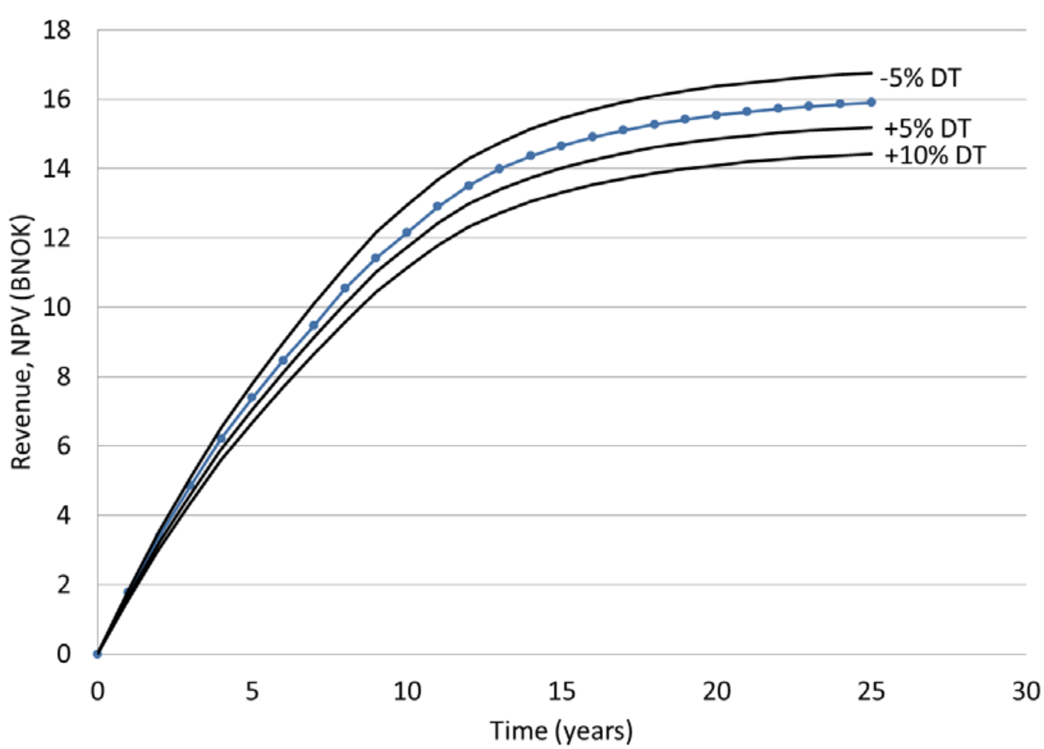

Figure 28. Sensitivity to downtime, subsea compression case

The lack of information available (definite annual expenditures, expected future development of cost of capital rate and oil & gas prices, namely), warrants further investigation.

The fact that the window of operations (or lifespan of the field) is significantly longer for Case 2 than Case 3, which in turn is longer than for Case 1, representing larger expenditures in terms of platform costs, salaries, etc., will have to be considered before making a final decision; however, without further information, it is impossible to provide more accurate figures.

The option of implementing a subsea compressor and reducing the inlet pressure of the separator is still open. Doing so can be expected to increase the field's expected plateau length significantly, and as such, generate additional profits. For the sake of this analysis, however, the option of reducing the separator pressure has not been considered.

All this taken into consideration, based on these calculations, improving recovery by the means of this subsea compressor assembly is likely to be the most profitable option.

Production of Wet Gas

In order to assess the impact of the dry gas assumption for the pressure losses calculated in the previously studied cases, a model in Aspen HYSYS ® was implemented. This model included the material balance equation and the inflow performance relationship (see Appendix) in a spreadsheet while the rest of the pressures were determined by simulation of the tubing in the wells and the pipeline from the templates to the platform, see Figure 29.

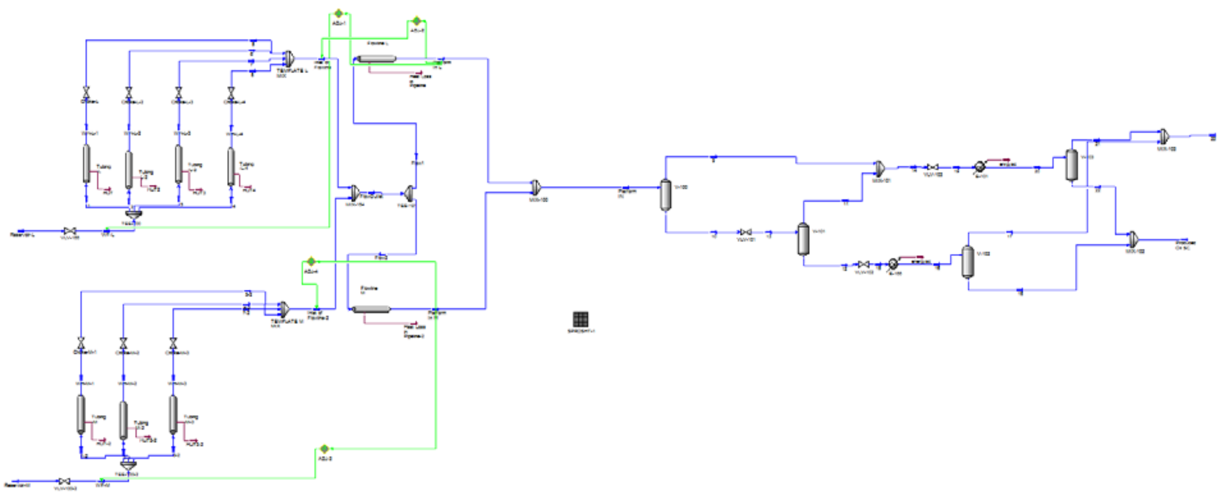

Figure 29. Aspen HYSYS ® flowsheet for the simulated model

The developed model is a representation of the natural depletion case, but the results can be extended to the compressor case since the pressures are calculated in a similar manner. Simulating the subsea compression case implied solving a network in HYSYS and it was a rather long iterative procedure for the purpose of this project.

Data for tubing, pipeline and composition of the gas was obtained from Statoil and is shown in the following set of tables. Table 5 presents the gas composition in molar percentage. Table 6 the required data for simulation of the well tubing while Table 7 and Table 8 present the data for the pipeline simulation and its profile respectively.

Table 5. Gas composition for HYSYS simulation

Component	Mole %
Nitrogen	0,24
Carbon Dioxide	1,56
Methane	86,10
Ethane	5,55
Propane	2,10
i-Butane	0,29
n-Butane	0,64
i-Pentane	0,20
n-Pentane	0,26
n-Hexane	0,32
Cyclopentane	0,08
Benzene	0,12
Cyclohexane	0,14
n-Heptane	0,23
Mcyclohexane	0,19
Toluene	0,20
n-Octane	0,24
E-Benzene	0,02
M-Xylene	0,10
O-Xylene	0,03
n-Nonane	0,18
C10+	1,21
C10+ Properties	
Molecular Weight	200
Ideal liquid density (kg/m^3)	814

Table 6. Tubing data for HYSYS simulation

Inner Diameter	0,1548 m
Outer Diameter	0,1778 m
Length	3000 m
Elevation Change	0 m
Material	Mild Steel
Roughness	4,57E-05 m
Pipe Wall Conductivity	45 W/m.°C
Surrounding temperature	60 °C
Overall HTC	2 W/m^2.°C
Flow correlation	Aziz, Govier and Fogarasi

Table 7. Pipeline data for HYSYS simulation

Inner Diameter	0,3556	m
Outer Diameter	0,375	m
Length	See profile	-
Elevation Change	See profile	-
Material	Mild Steel	
Roughness	4,57E-05	m
Pipe Wall Conductivity	10	W/m.°C
Surrounding temperature	5	°C
Overall HTC	0,5	W/m^2.°C
Flow correlation	Beggs and Brill (1979)	

Table 8. Pipeline profile for HYSYS simulation

Length/Equivalent Length (m)	9000	5000	260
Elevation Change (m)	0	-80	260

The results of studying the field production including pressure drop due to the condensate are represented in two main figures which compare the natural depletion pressure profiles with the profiles obtained from this simulation. Figure 30 shows the comparison for template L while Figure 31 shows the case for template M.

As can be seen from the plotted pressures, the largest difference was in the node at Ptemplate, which means that the pressure loss in the 14-km pipeline was largely underestimated by the dry gas assumptions, however it is important to highlight the fact that the assumption of horizontal pipeline could also represent a significant contribution to this difference.

Two things stand out from these comparative figures, the first is that although there is a noteworthy difference in the pressure values for some of the nodes, the trend is relatively similar when comparing the dry and wet gas cases; this could be taken as an important input for the studies done earlier in this report since it shows that the values might have some uncertainties but the behavior of the field is well predicted by the dry gas assumptions.

The second thing is that apparently, after year 2020 the flow from template M is so small that the gas velocity drops to enter the transition zone between friction dominated and gravity dominated pressure drop, this means that the pressure drop cannot be reduced by means of flow reduction anymore, see Figure 32.

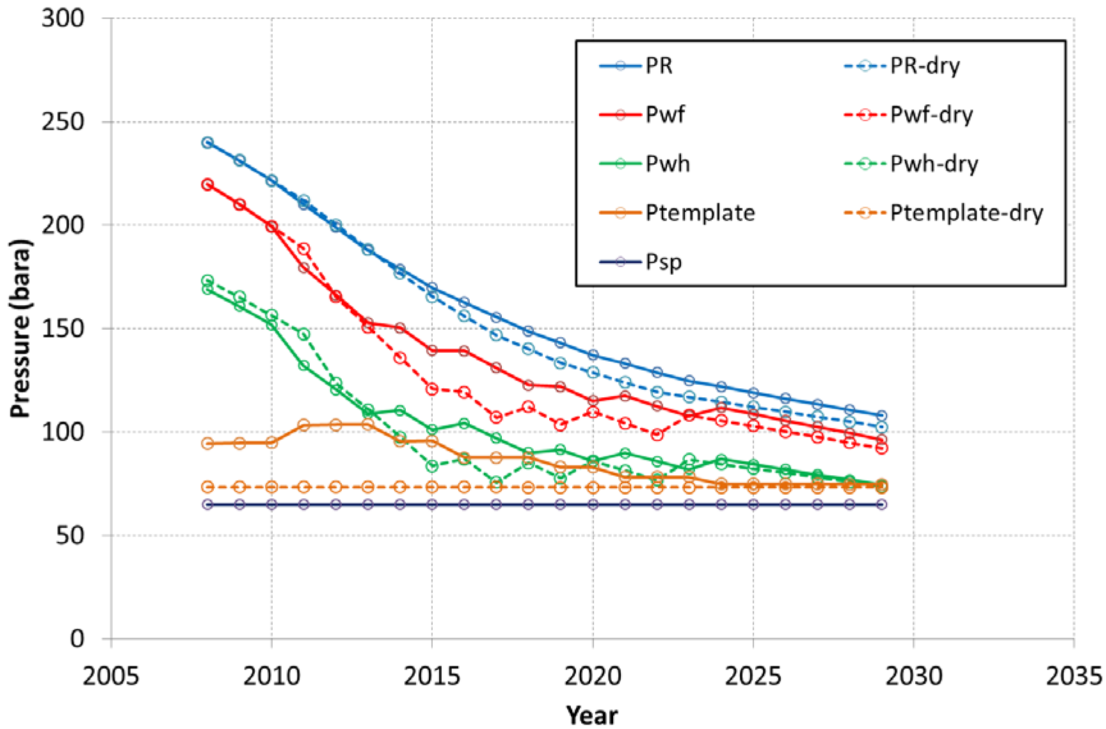

Figure 30. Pressure profile L-template, dry gas vs wet gas

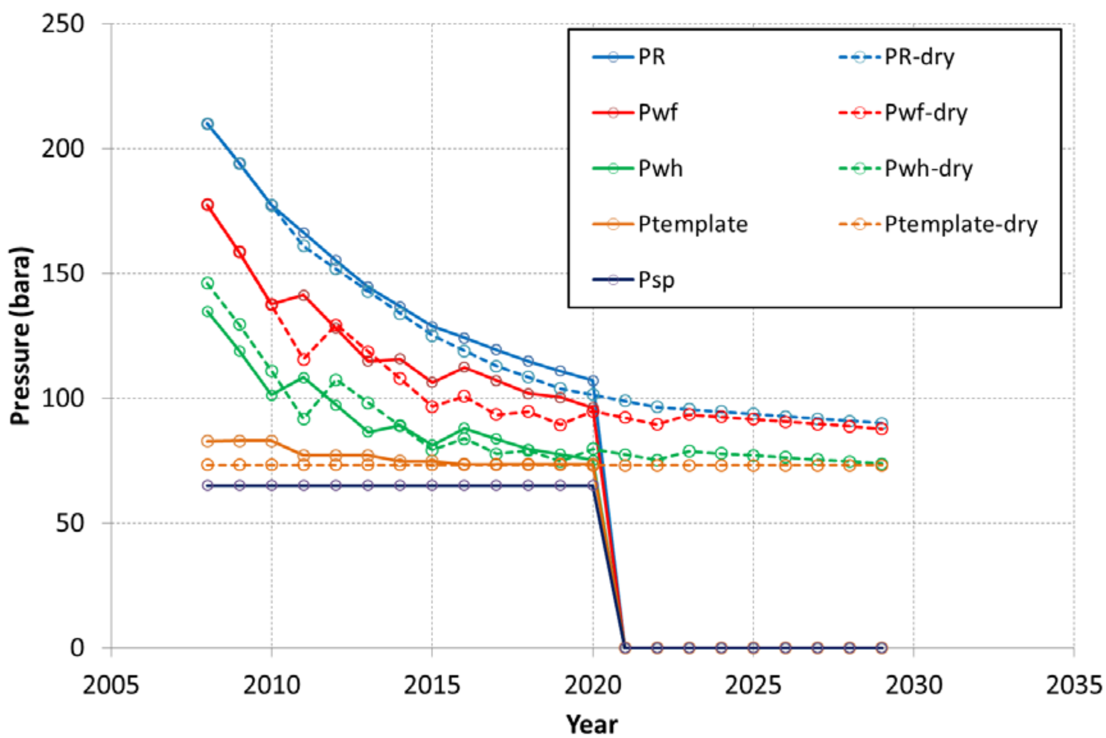

Figure 31. Pressure profile M-template, dry gas vs wet gas

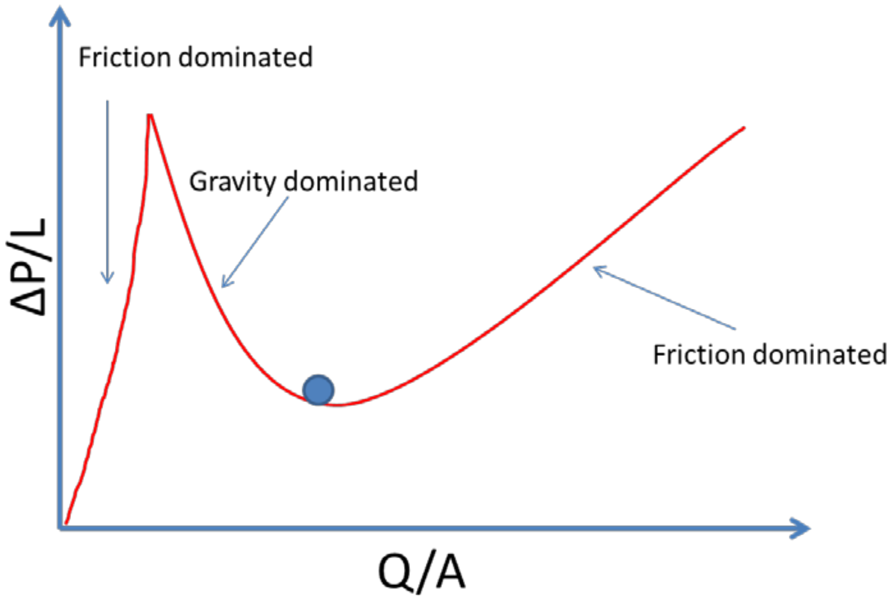

Figure 32. Pressure loss in multiphase flow, vertical pipes [3]

Liquid Loading of Gas Wells

As the pressure in the well drops, eventually, the pressure of the flowing gas will drop below the dew point (the pressure threshold where the first drop of liquid forms in the gas), meaning that droplets of liquid will start forming. The density of these droplets is significantly higher than that of the flowing gas, and as such, requires greater energy to be lifted out of the well. At some point, the velocity of the flowing gas will drop below the critical velocity of these droplets (the velocity required to lift named droplets out of the well).

Left unchecked, liquid may start accumulating in the bottom of the well, and as the liquid level increases, eventually, the liquid level may rise above the producing reservoir level. When this occurs, pressure losses can be observed in the production line, as the gas bubbles through liquid, causing a downward spiral of ever increasing liquid accumulation, up until the point where the pressure exerted by the accumulated fluids equals the pressure of the reservoir, halting production completely.

Liquid Loading is a phenomenon that can cause significant problems in producing gas wells. The objective of this analysis is to determine whether unloading measures will have to be implemented in order to ensure the productivity of templates L & M at the Gullfaks South Satellite.

R.G. Turner developed an equation that can be used to estimate onset of liquid loading in producing gas wells. The critical slip velocity of liquid droplets can be calculated as a function of interfacial tension between gas and liquid, and the difference in densities of gas and liquid, multiplied by a constant. The value of this constant has been the subject of much debate, and as such, has been challenging to determine.

Turner's Equation: $$u = C\frac{\sigma^{\frac{1}{4}}(\rho_L - \rho_g)^{\frac{1}{4}}}{\rho_g^{\frac{1}{2}}} \qquad (1)$$

Density of oil from gas is found by taking values of densities from IPT-Matbal, relating them to pressure, and performing polynomial regression, thereby finding representative equations for density of oil as a function of pressure for both L & M templates as follows.

L : $\rho_{oil\ from\ gas} = 3E\text{-}08p^4 - 2E\text{-}05p^3 + 0{,}0031p^2 - 0{,}1135p + 786{,}62$ (2)

M: $\rho_{oil\ from\ gas} = 2E\text{-}08p^4 - 5E\text{-}06p^3 - 0{,}0005p^2 + 0{,}2202p + 778{,}54$ (3)

In order to simplify the analysis, the following assumptions and considerations were taken:

- Density of water is constant, taken at T=98 °C and T=82 °C for template L and M respectively (assumed temperature drop of 30 °C from reservoir to wellhead)
- Liquid is to be produced primarily from gas (Liquid production from reservoir negligible)
- Compressibility of oil and water negligible
- Pressure below dewpoint pressure ($p < p_d$) for the entire production interval
- The compressibility factor for gas is obtained from the previously performed material balance in IPT-MATBAL

The provided charts, Figure 33, Figure 34, Figure 35 and Figure 36 have been generated using four different values for the constant in Turner's equation, starting with Petroleum Experts' recommended value of C=2,04 (in metric units), and adding three additional values, intended to illustrate how sensitive the results are with regards to this uncertainty.

In order to provide a conclusion from this study, the value of the constant C=2,04 will be used. As can be observed in Figure 33 and 34, it seems likely that the wells making up template L will experience water and condensate accumulation in the well in the later years of production. On the other hand, the calculations indicate that water loading will take place in Template M from the very start of this production interval, and that condensate loading will occur after nine years of production.

In the real world, one might not detect any indications that this is, in fact, happening (no pressure loss observed). One significant source of uncertainty is most certainly the estimate of the constant value, but depending on the geology of the formation, low pressure zones located below the producing reservoir layers may be absorbing liquid as it accumulates.

If pressure loss due to liquid loading is detected, the well can be unloaded by installing velocity strings (a smaller diameter tube is lowered into the well, causing the velocity of the flowing fluids to increase), or one might inject deliquifying agents into the well, in order to prevent liquid from ever coalescing from the gas.

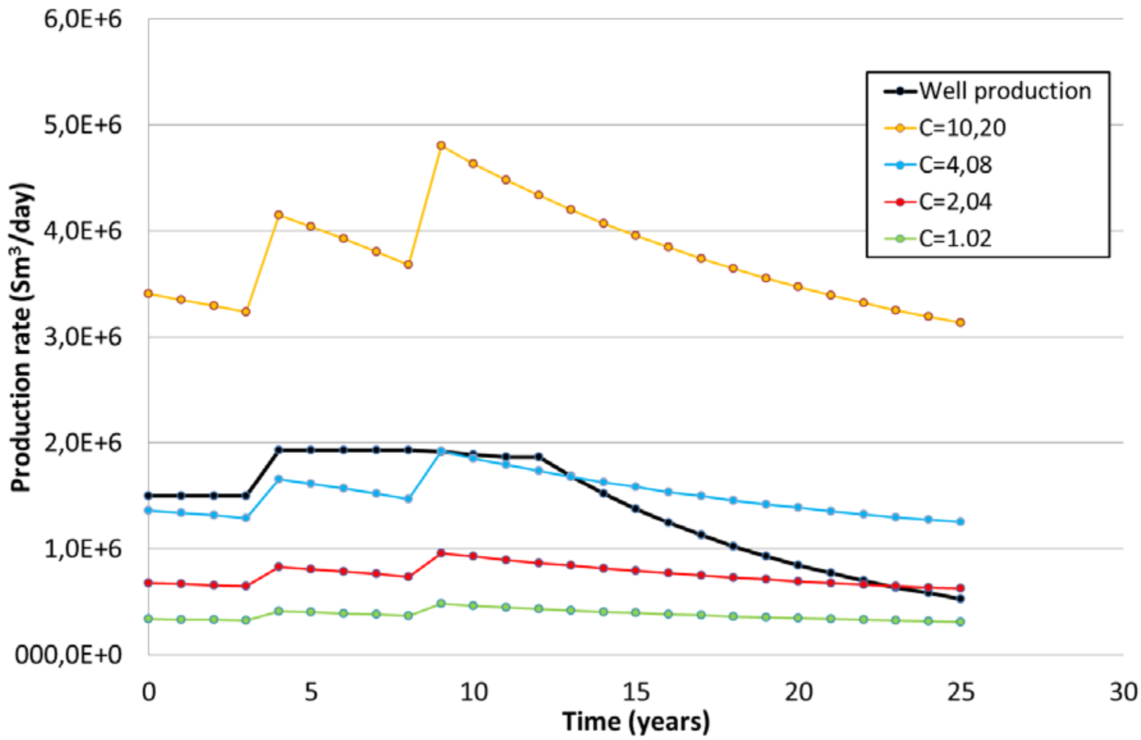

Figure 33. Condensate loading of template L wells

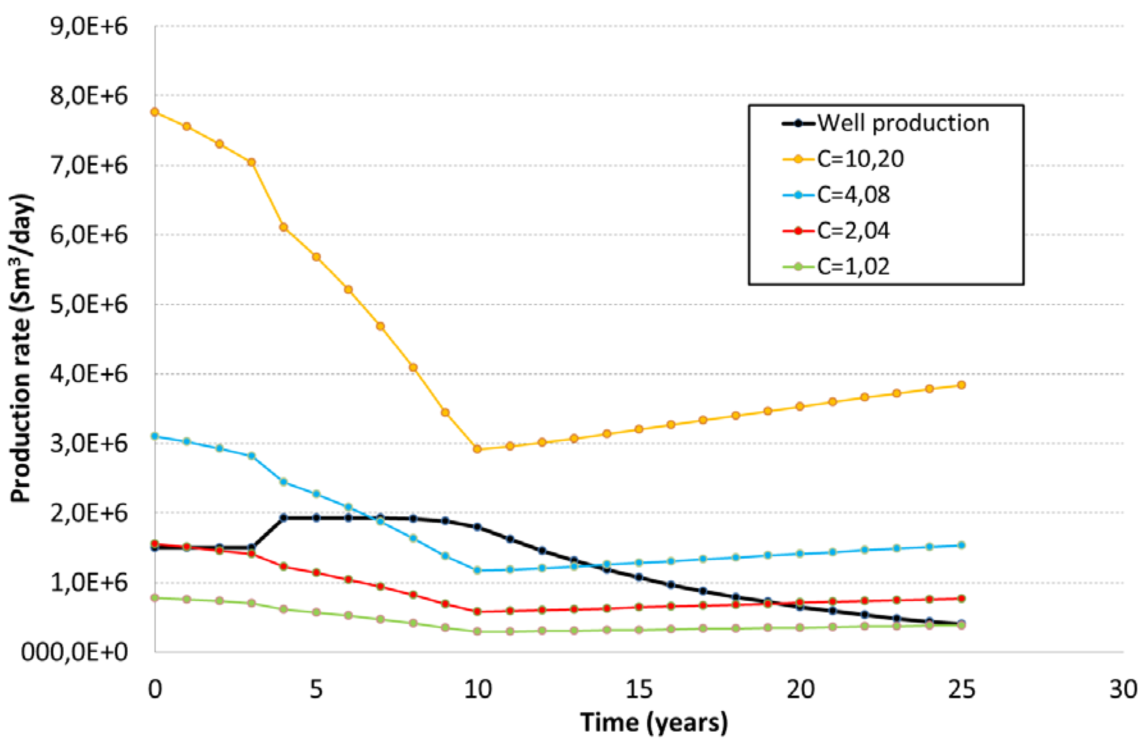

Figure 34. Water loading of template L wells

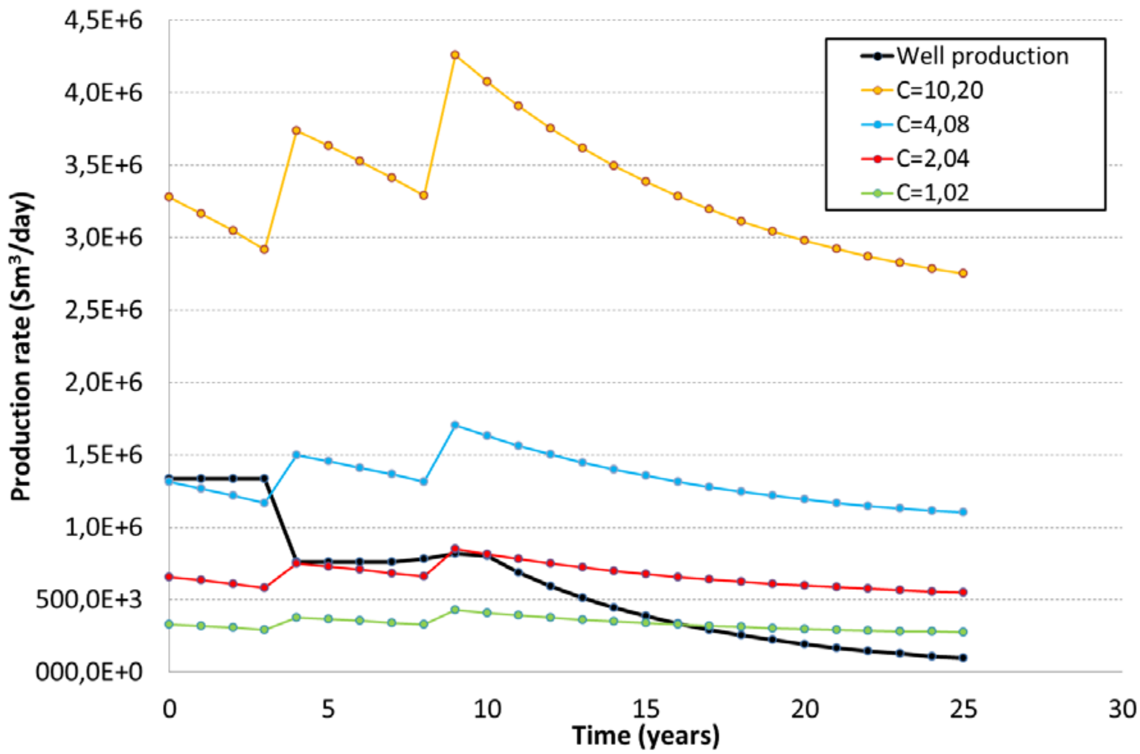

Figure 35. Condensate loading of template M wells

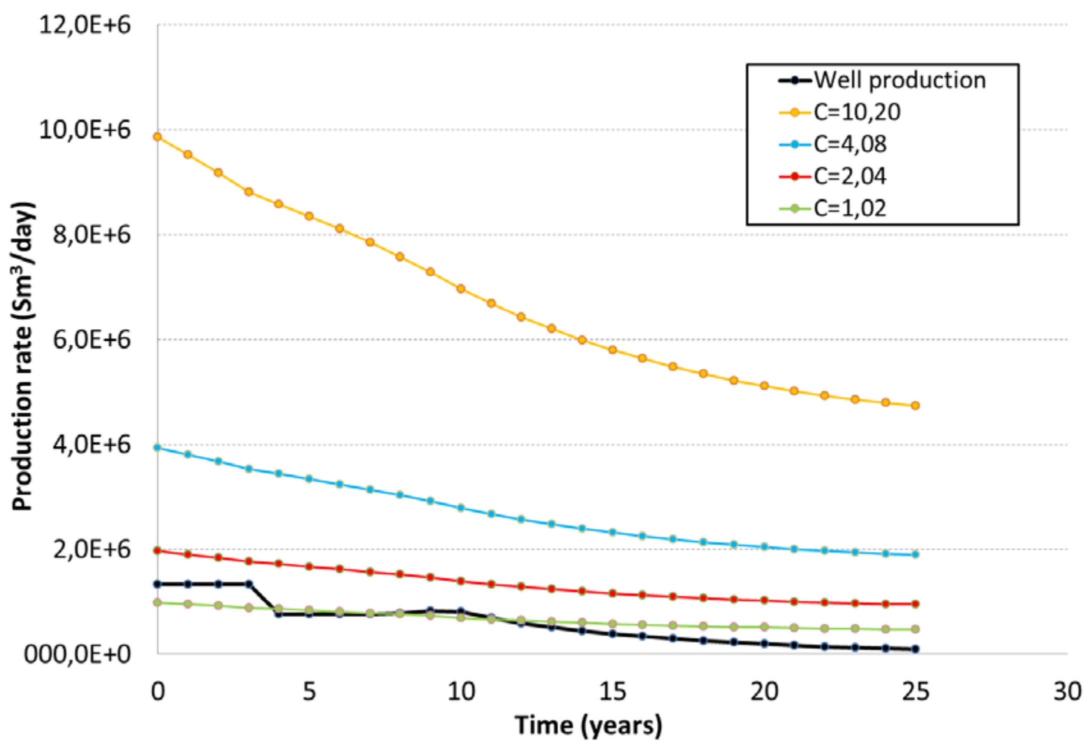

Figure 36. Water loading of template M wells

Hydrate Risk Analysis

Hydrates are crystalline compounds which occur when gas and water mix under certain temperature and pressure conditions [4] . Hydrates may be one of the largest problems with regards to flow assurance in multiphase pipelines, as these may cause blockage of the lines. Based on this, a hydrate risk analysis is performed in order to measure the possibility of hydrate formation during production of Gullfaks South.

In order to assess the hydrate risk, a correlation developed by Makogon in 1988 [5] was used. It is a very simplified correlation which is dependent on the specific gas gravity. The equation is as following

$$\ln P = 2{,}3026\beta + 0.1144(T + \kappa T^2) \qquad (1)$$

$$\beta = 2.681 - 3.811\gamma + 1.679\gamma^2 \qquad (2)$$

$$\kappa = -0.006 + 0.011\gamma + 0.011\gamma^2 \qquad (3)$$

Where γ is the specific gravity, T is temperature in °C and β and κ are constants. The specific gravity was given in the data for the field (see Table 1). By applying γ=0.66 the hydrate curve was plotted. The hydrate formation zone is to the left of the hydrate curve, in the high pressure, low temperature area, see Figure 37.

From the previously done simulations in HYSYS, the pressure and temperature profile for the 14" pipelines were obtained. The first year of operation (2009) and the last year of operation were considered key cases to be studied for the hydrate risk. The first year the pipeline will have the highest pressure as well as the largest pressure drops due to friction. While for the last year, the pipeline is expected to have the largest heat transfer with the surrounding water due to the small flow rate.

By evaluating the hydrate risk for these years (first and last) in the natural depletion case, it is also possible to assess the hydrate risk for the subsea compression case, since once the compressor is installed the pressures in the pipeline will not exceed the ones during the first year of production and the temperature will be higher due to the temperature rise in the compressor.

The pipelines were assumed to be insulated, and a low heat transfer coefficient of 0,5 $W/m^2.K$, was estimated, the results for the insulated pipeline are shown in Figure 38. The heat transfer coefficient was assumed to be low based on a paper under the title "Boosting the Heating Capacity of Oil-Production Bundles Using

Drag-Reducing Surfactants" by E. Sletfjerding et al, 2003, where the pipeline bundle for the field was described as heat insulated. In order to have a reference, a non-insulated pipeline was also considered with an overall heat transfer coefficient of 3,0 $W/m^2.K$, see Figure 39.

Hydrate risk before entering the pipeline was also assessed, especially for the subsea compression case where a passive cooler is installed upstream the compressor. According to Statoil and Framo Engineering staff (from the visit to Bergen) this cooler is designed to cool the gas down to a temperature between 20 and 25 degrees Celsius. From Table 4 it is possible to find that the highest pressure at the compressor suction is 69 bar; with this pressure and a temperature of 20 °C the hydrate risk for this case is assessed and presented in Figure 39. Additionally, since installing the compressor might require the field to be shut down, a worst-case scenario where the pipeline reaches seabed temperature with shut-in wells (65 bar) is investigated, this is also shown in Figure 39.

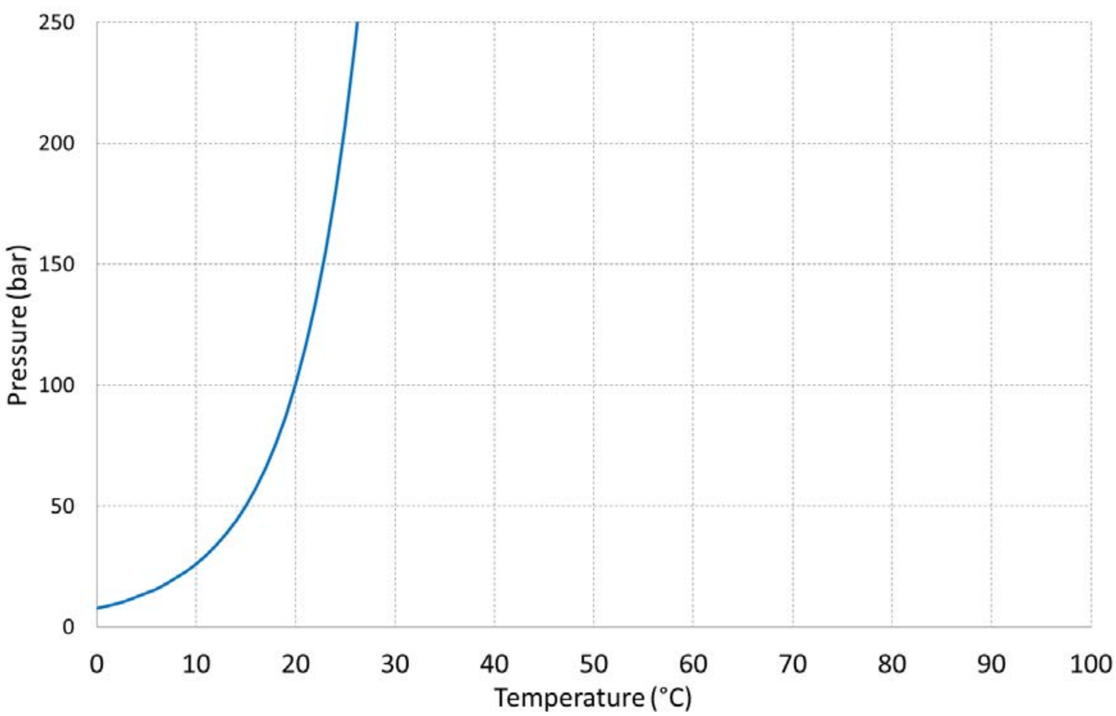

Figure 37. Hydrate curve for Gullfaks South

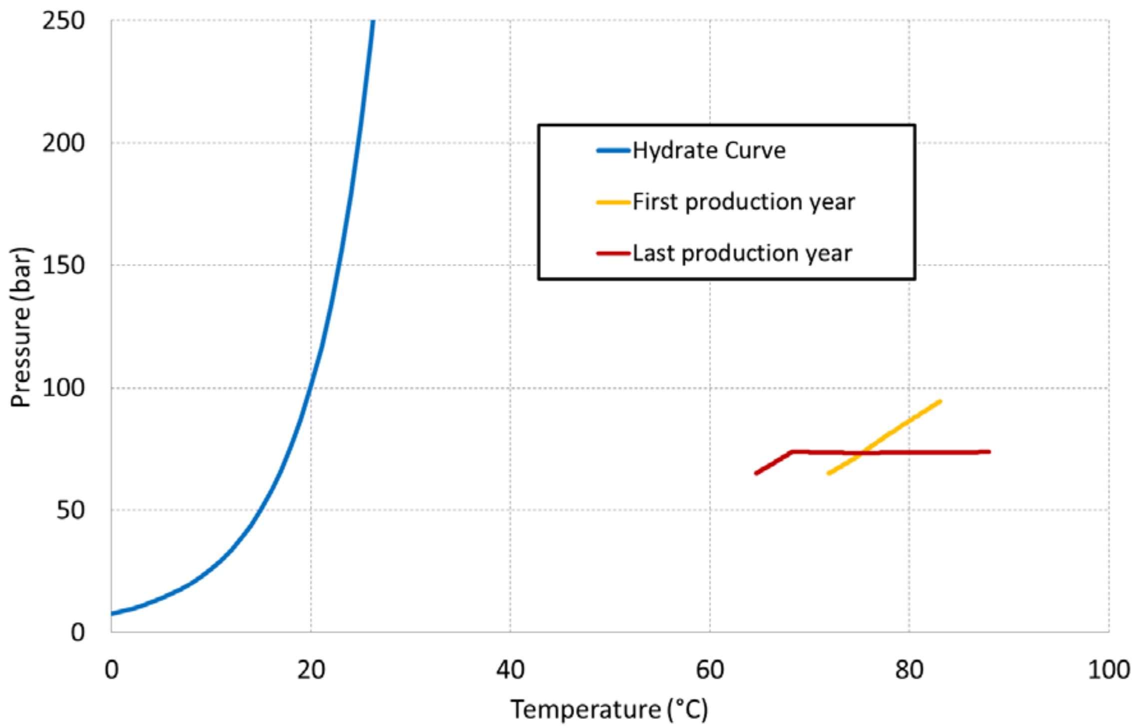

Figure 38. Hydrate risk first and last production year, insulated pipe

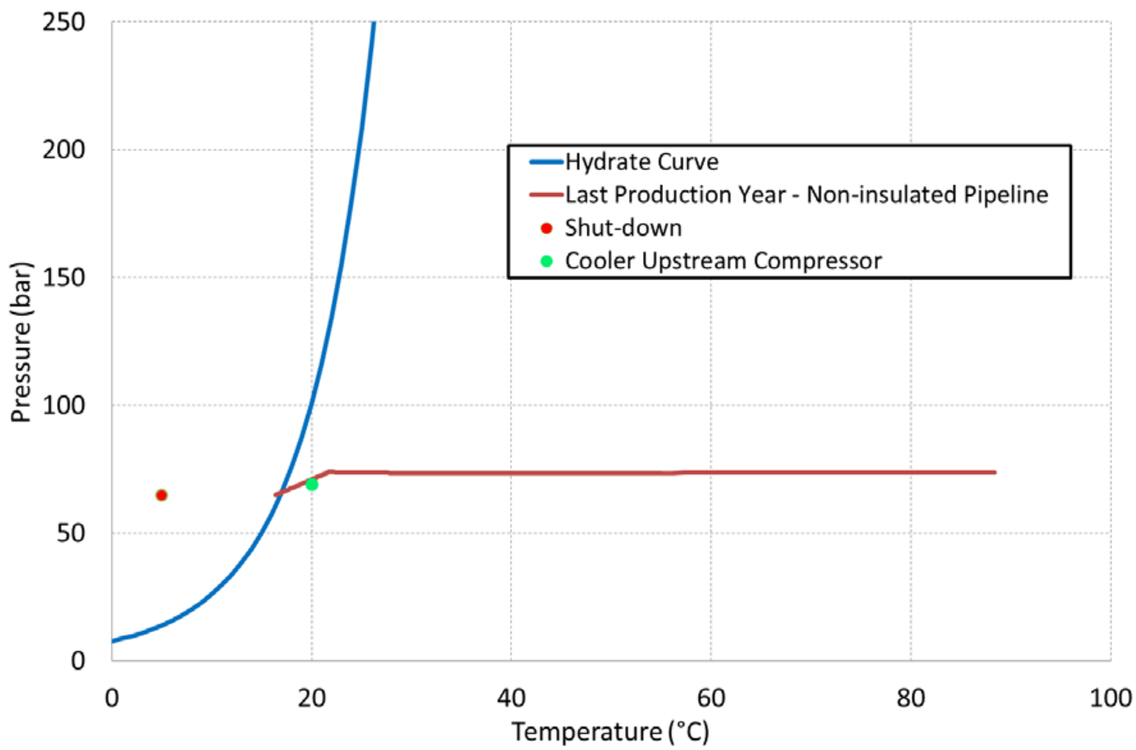

Figure 39. Hydrate risk for shut-down, compressor cooler and non-insulated pipe

As can be seen from Figure 38, hydrate formation does not represent a problem during normal operation of the field, neither for the natural depletion nor for the subsea compression case. However, if the field is expected to be shut-down during a significant period of time, or if the estimation of heat transfer coefficient presented in this report seems too optimistic, hydrate formation should be studied with more detail, see Figure 39. No hydrate formation issues with the passive cooler upstream the compressor were found either.

Conclusions

Based on well configuration calculations, it is not recommended to alter the template configuration studied as the base case for this report where the flows from L and M templates are commingled at the towhead and distributed evenly among the two 14 inch pipelines.

The field production calculations indicate that adding a subsea compressor assembly to the assigned Gullfaks South templates such as the one used as basis for this report can be expected to yield an increase in reservoir recovery factor from 57% to 75% when compared with the option of continuing producing by natural pressure depletion. However, the reduction in separator pressure produces a recovery rate up to 79%, which suggests (without looking at the related revenues) that the best case scenario would be the implementation of a subsea compressor followed by a reduction in the separator pressure.

NPV calculations support the decision to install the subsea compressor, since it produces larger revenues in shorter time span, although the uncertainties surrounding the project warrants further investigation into the matter. The major unique uncertainty in this case is the project's sensitivity to downtime, as the compressor assembly is unqualified and untested outside a laboratory. However, the leap this project represents with regards to available technology intended to increase recovery is a good argument to go ahead, even if it might prove less profitable than the next best option, as it is quite clear that the potential is significant.

The dry gas assumption seems to give a good representation of the general behavior of the field. However, the actual pressure loss while producing will be greater than the estimates presented in this report, and this will have a negative impact on production, and therefore, the profitability of the project. All other things being equal, though (all the cases evaluated are based on the same assumptions, and therefore it can be assumed that all of them are affected to a comparable degree by deviations), it is not expected that this will cause great discrepancies to the reached conclusions when comparing the different options.

Based on estimates provided in this report, it seems apparent that pressure drop caused by liquid loading of the gas wells may occur at different times during the life of the field, impairing production. Efforts should be made to evaluate unloading alternatives, the impact they may have on production with regards to flow restrictions, and the time it may take to implement them. Hydrate formation was not found to be an issue during production, especially since the pipeline is well insulated; yet in case of shut-down the temperature could reach the hydrate formation zone.

Recommendations

- Historical data, actual production and pressure figures would be helpful for further tuning of the developed model with the actual Gullfaks South Satellite field
- The study of different scenarios for the implementation of the separator pressure reduction might give a better idea of the best instance to apply this modification.
- The reliability of the equipment proved to be a critical factor for the profitability of the project, therefore a risk-assessment study regarding the operation of the compressor would be helpful to support the execution of this project

References

1. Administration., U.S.E.I., International energy outlook and projections2011, Hauppauge, N.Y.: Nova Science Publishers. vii, 453 p.

2. British Petroleum Company., BP statistical review of world energy, 2011, British Petroleum Co.: London. p. v.

3. Nydal, O.J, Multiphase Transport Handouts, Trondheim, Spring 2012

3. Bratland, Ove, Pipe flow 2 – Multiphase Flow Assurance, 2010. Available online: http://www.drbratland.com/PipeFlow2/PipeFlow2Multi-phaseFlowAssurance.pdf

4. D.L. Katz, R.L. Lee, Natural Gas Engineering, McGraw-Hill, New York, 1990

5. C. Whitson, M. Brulé, Phase Behavior, Society of Petroleum Engineers, Inc., Texas, 2000

Please notice that no further references were used due to the continuous teaching assistance that we were given during the development of this project. Most of the studied cases were done under the supervision of Prof. Michael Golan or one of the Ph.D. students at the Department of Petroleum Engineering and Applied Geophysics.

Appendix

- **Equations of the pressure loss and material balance in Excel**

Material Balance, dry gas, tank model:

$$p_R = p_i\left(\frac{z_R}{z_i}\right)\left(1-\frac{Gp}{G}\right)$$

Z factor estimated using a provided Excel programmed function for Standing's Correlation.

Inflow equation, inflow performance relationship (IPR):

$$q_{gsc} = C_R\left(p_R^2 - p_{wf}^2\right)^n$$

Horizontal flowline/pipeline equation:

$$q_{sc} = C_{FL}(p_{in}^2 - p_{out}^2)^{0.5}$$

Tubing equation, tubing performance relationship (TPR):

$$q_{gsc} = C_T\left(\frac{p_{in}^2}{e^s} - p_{out}^2\right)^{0.5}$$

- **IPT-MATBAL**

For the solution using IPT-MATBAL, a black oil property table covering the whole range of reservoir pressures has to be provided. These black oil properties were estimated using Aspen HYSYS ® in a simulation of a so-called PVT test, see Figure 40 for the simulation flowsheet. Table 9 shows the black oil table for template L while Table 10 shows the values for template M; notice that although the composition for both templates/reservoirs is the same, the temperatures are different and thus different values are obtained.

The solving procedure of IPT-MATBAL is based on SPE's Phase Behavior monograph by Whitson and Brulé [6] where an iterative procedure is proposed to reach a solution for gas-condensate reservoir material balance. A snapshot of this procedure is taken from the monograph and shown in Figure 41.

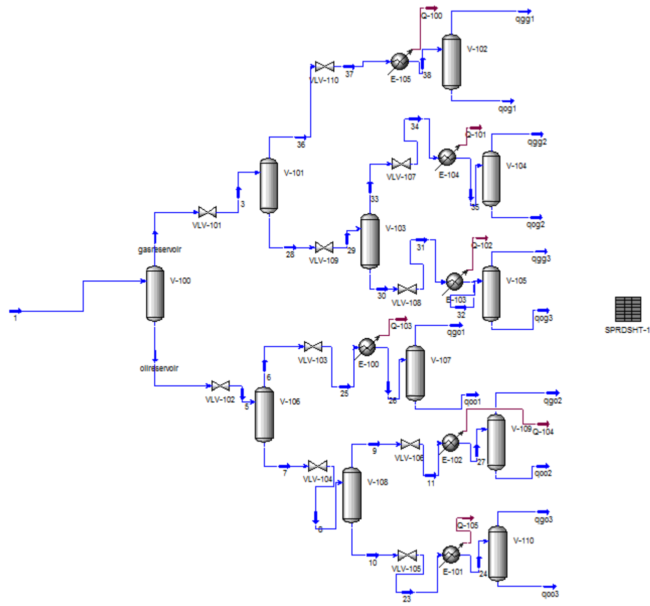

Figure 40. HYSYS flowsheet for PVT test simulation

Table 9. Black Oil property table, template L

p	B_o	B_g	R_s	r_s	muo	mug	denog	denoo	gammao	dengo	dengg	gammag
[bara]	[m^3/Sm^3]	[m^3/Sm^3]	[Sm^3/Sm^3]	[Sm^3/Sm^3]	[cp]	[cp]	[Kg/m^3]	[Kg/m^3]	<empty>	[Kg/m^3]	[Kg/m^3]	<empty>
240	1,717224107	5,80E-03	184,294	1,09E-04	0,180858199	2,27E-02	796,2747217	803,3837707	0,991151117	0,892901661	0,823923735	1,083718823
220	1,639153718	6,25E-03	160,8476536	8,82E-05	0,196290432	2,16E-02	795,8843507	803,0850639	0,991033686	0,900048917	0,824723518	1,091334122
200	1,572472152	6,81E-03	139,5791015	7,12E-05	0,211803407	2,06E-02	795,5829704	802,7800523	0,991034802	0,907547893	0,825424904	1,099491776
180	1,509701084	7,51E-03	120,116028	5,71E-05	0,228010466	1,97E-02	795,3092988	802,4849397	0,991058224	0,915386687	0,82596294	1,108266052
160	1,450090073	8,41E-03	102,1737441	4,58E-05	0,245113321	1,89E-02	794,9496589	802,2243109	0,990931898	0,923519479	0,826307292	1,117646532
140	1,394065002	9,59E-03	85,53537097	3,69E-05	0,263262422	1,81E-02	794,343959	802,03468	0,990410987	0,931853092	0,826483026	1,127492112
120	1,341947233	1,12E-02	70,04082549	3,03E-05	0,28270262	1,74E-02	793,3169651	801,9693493	0,989211079	0,940230473	0,826580154	1,137494614
100	1,293813696	1,35E-02	55,58170352	2,57E-05	0,303863548	1,68E-02	791,7342065	802,1056382	0,987069743	0,94841359	0,826748719	1,14716064
80	1,249615042	1,69E-02	42,10118893	2,30E-05	0,32745486	1,62E-02	789,5782944	802,5570277	0,983828273	0,95607784	0,8271865	1,15581896
60	1,208863169	2,27E-02	29,49760401	2,20E-05	0,354596746	1,57E-02	787,3525975	803,4544876	0,979959176	0,957270883	0,82826025	1,155760985
40	1,171200457	3,45E-02	17,74563978	2,36E-05	0,388961135	1,53E-02	785,8864603	805,0413288	0,976206354	0,930934775	0,830337266	1,121152588
20	1,13897215	6,99E-02	7,516354664	3,39E-05	0,445594625	1,50E-02	785,5569602	808,0526794	0,972160578	0,877618449	0,832388535	1,054337502

Table 10. Black Oil property table, template M

P	B_o	B_g	R_s	r_s	muo	mug	denog	denoo	gammao	dengo	dengg	gammag
[bara]	[m^3/Sm^3]	[m^3/Sm^3]	[Sm^3/Sm^3]	[Sm^3/Sm^3]	[cp]	[cp]	[Kg/m^3]	[Kg/m^3]	-	[Kg/m^3]	[Kg/m^3]	-
240	1,689905857	5,47E-03	192,2363529	9,75E-05	0,198809161	2,27E-02	789,7681357	801,8105886	0,984980926	0,886257215	0,817127141	1,084601368
220	1,620158328	5,89E-03	168,6084158	7,74E-05	0,214668728	2,15E-02	789,2535034	801,3874141	0,98485887	0,894192156	0,818582268	1,092366878
200	1,555393266	6,42E-03	147,0426539	6,03E-05	0,231081125	2,05E-02	789,1548478	800,9367445	0,985289854	0,902724351	0,820024241	1,100850811
180	1,49373295	7,08E-03	127,1752935	4,59E-05	0,248314321	1,95E-02	789,5472782	800,4762674	0,986346892	0,911886623	0,821314018	1,11027768
160	1,435262626	7,93E-03	108,7244461	3,43E-05	0,266532915	1,86E-02	790,3951537	800,034581	0,987951237	0,921680996	0,822305198	1,120850261
140	1,380239746	9,05E-03	91,47439562	2,54E-05	0,285963872	1,78E-02	791,4495308	799,6556284	0,989737961	0,932063426	0,822913969	1,132637749
120	1,32874722	1,06E-02	75,26803776	1,89E-05	0,306990694	1,71E-02	792,226768	799,4043982	0,991021278	0,942925322	0,823205324	1,145431516
100	1,280738773	1,27E-02	60,00438092	1,46E-05	0,330246168	1,64E-02	792,1556846	799,3752669	0,990968469	0,954074173	0,823418747	1,158674339
80	1,236149366	1,61E-02	45,63994877	1,21E-05	0,356753375	1,58E-02	790,8003133	799,7069111	0,988862672	0,965223766	0,823918753	1,171503576
60	1,194525722	2,16E-02	32,0871944	1,09E-05	0,388192468	1,53E-02	788,4924051	800,5692495	0,984914679	0,970723794	0,825250219	1,176278141
40	1,155575597	3,28E-02	19,34522598	1,13E-05	0,429852735	1,48E-02	786,2313996	802,2902826	0,9799837	0,950536036	0,828145283	1,147788987
20	1,121852422	6,67E-02	8,176890722	1,73E-05	0,503812049	1,44E-02	782,7629372	805,8813677	0,971312861	0,905194891	0,832483846	1,08734229

Gas-Condensate Reservoir.

1. Specify $(\Delta G_p)_k$, total surface gas produced in scf/bbl of bulk volume.
2. Assume $(\overline{p}_R)_k$ and calculate PVT properties and porosity: $(B_o)_k$, $(R_s)_k$, $(\mu_o)_k$, $(\gamma^*_{\overline{o}})_k$, $(B_{gd})_k$, $(r_s)_k$, $(\mu_g)_k$, $(\gamma^*_{\overline{g}})_k$, and $(\phi)_k$.
3. Calculate oil saturation $(S_o)_k$ from Eqs. 7.39 through 7.41.

$$(S_o)_k = \frac{(A_g)_{k-1} - (\Delta G_p)_k - \left[\phi(1 - S_{wi})/B_{gd}\right]_k}{\left[\phi\left(R_s \gamma^*_{\overline{g}}/B_o - 1/B_{gd}\right)\right]_k}. \quad \ldots . \quad (7.46)$$

4. Calculate $(k_{rg}/k_{ro})_k$ from $(S_o)_k$.
5. Calculate $(A_o)_k, (A_g)_k, (E_o)_k$, and $(E_g)_k$.
6. Calculate ΔN_{po}, incremental surface oil produced from reservoir oil, where $\Delta N_{po} = \Delta G_p/\overline{E}_g$ and $\overline{E}_g = 0.5[(E_g)_k + (E_g)_{k-1}]$.
7. Calculate ΔN_p, incremental total surface oil produced, where $\Delta N_{po} = \Delta N_p/\overline{E}_o$ and $\overline{E}_o = 0.5[(E_o)_k + (E_o)_{k-1}]$.
8. Calculate the material-balance error,

$$\varepsilon = (A_o)_k - (A_o)_{k-1} + \Delta N_p. \quad \ldots\ldots\ldots\ldots\ldots\ldots \quad (7.47)$$

9. If ε is not sufficiently small, assume a new pressure $(\overline{p}_R)_k$ and redo Steps 2 through 8.

Figure 41. Solving gas-condensate reservoir material balance [6]

- **Compressor maps**

The compressor maps are shown only for the power curves as mentioned earlier in this report.

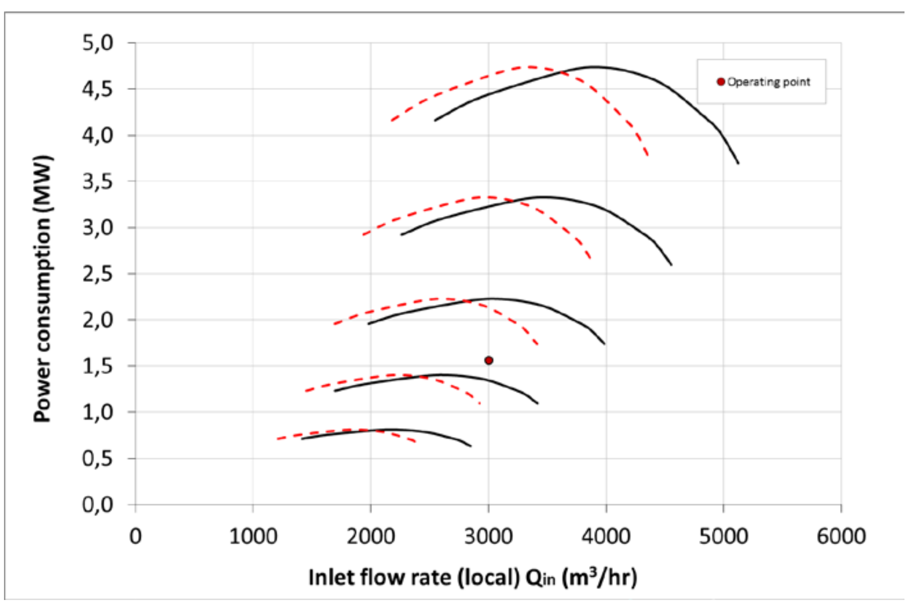

Figure 42. Compressor map, power, year 2016

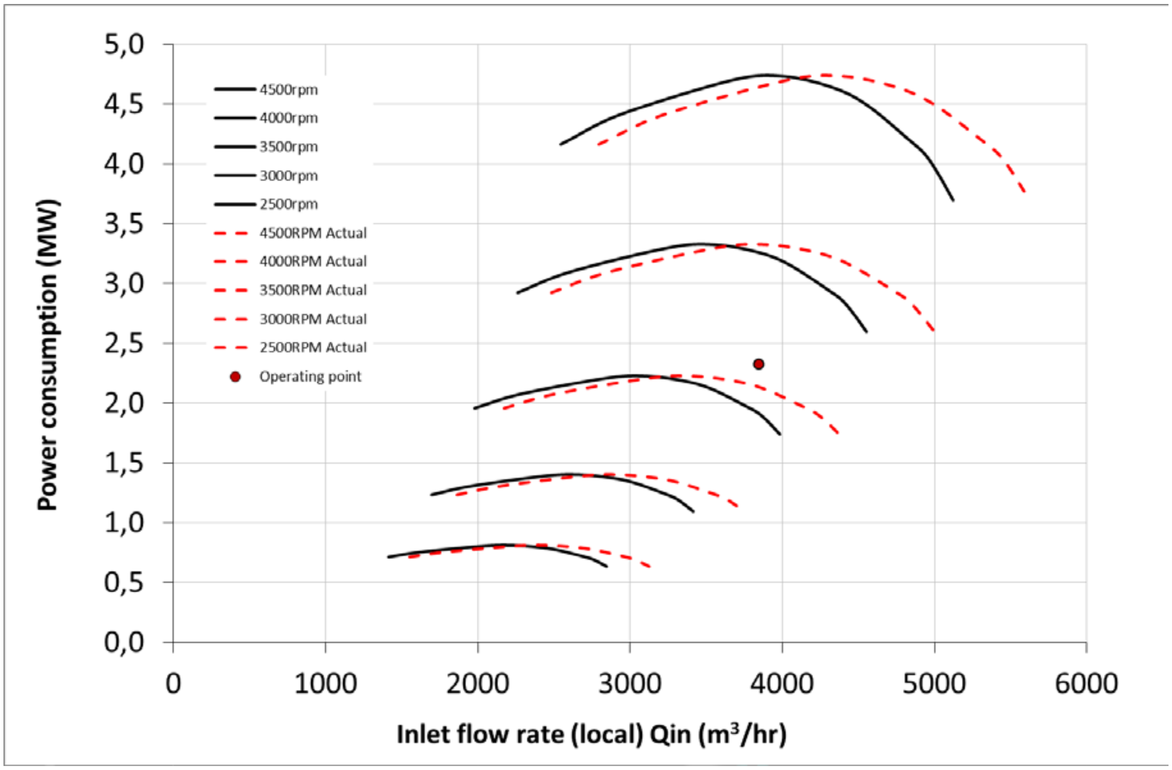

Figure 43. Compressor map, power, year 2017

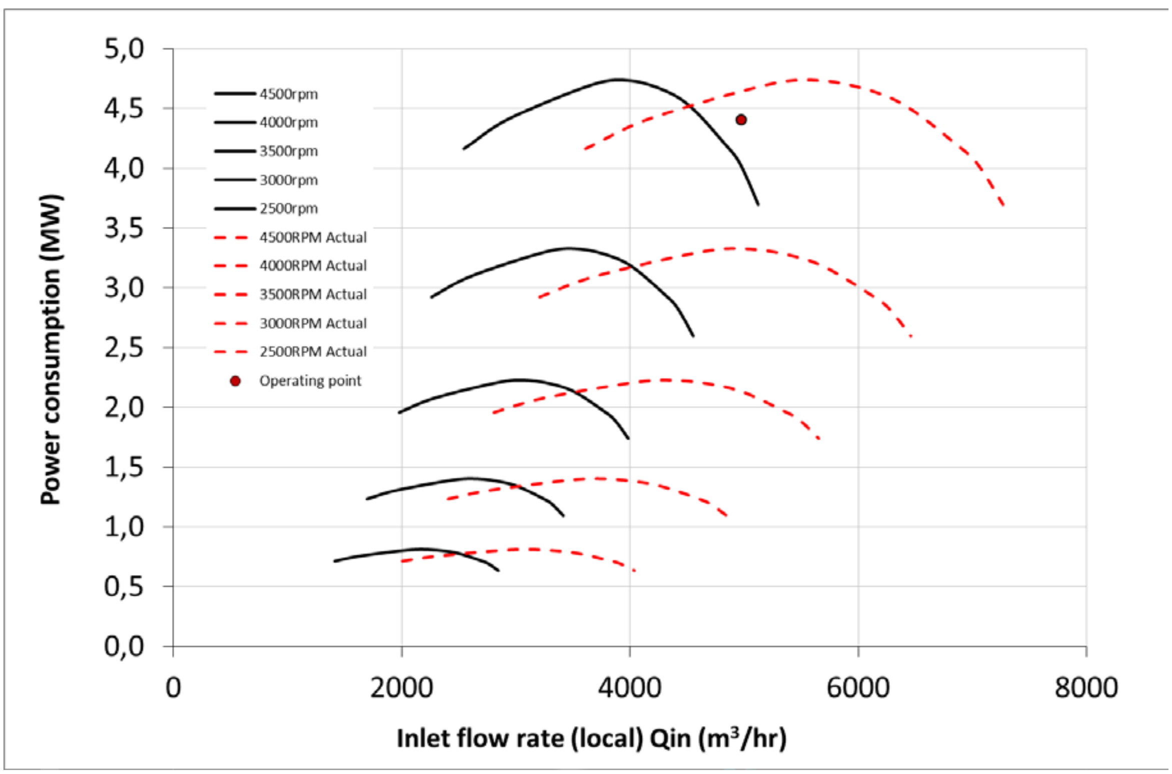

Figure 44. Compressor map, power, year 2018

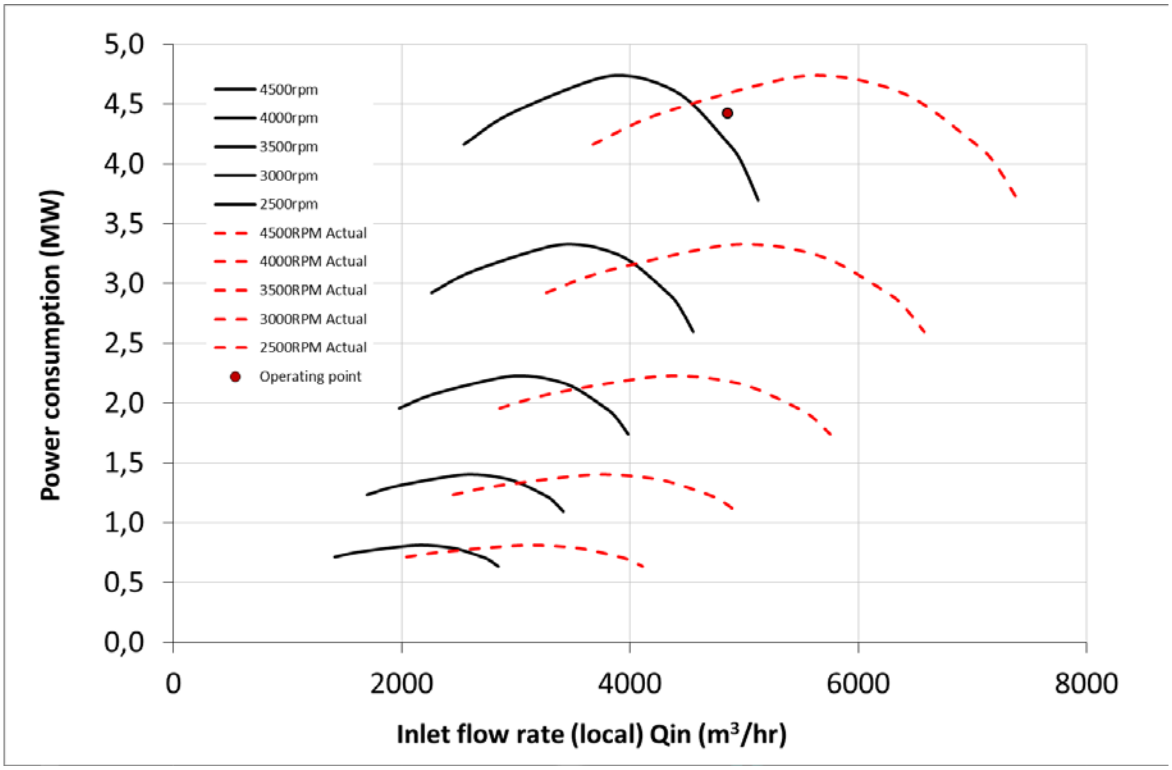

Figure 45. Compressor map, power, year 2019

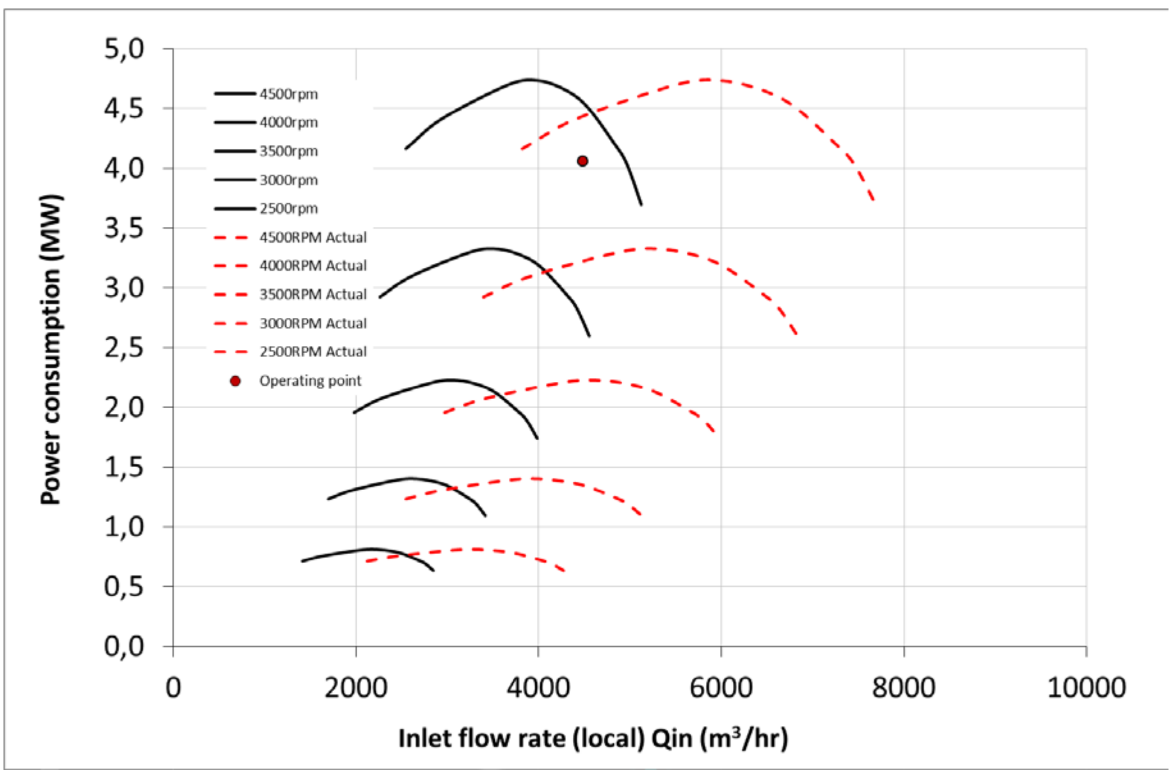

Figure 46. Compressor map, power, year 2020

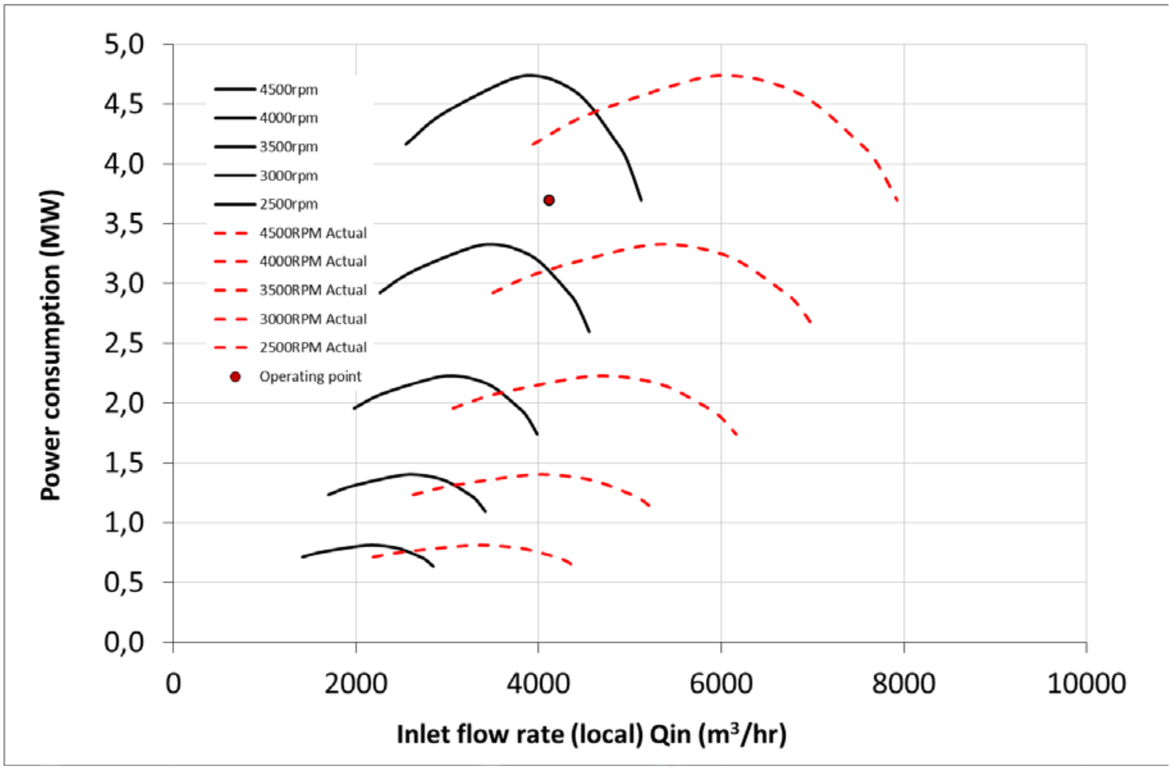

Figure 47. Compressor map, power, year 2021

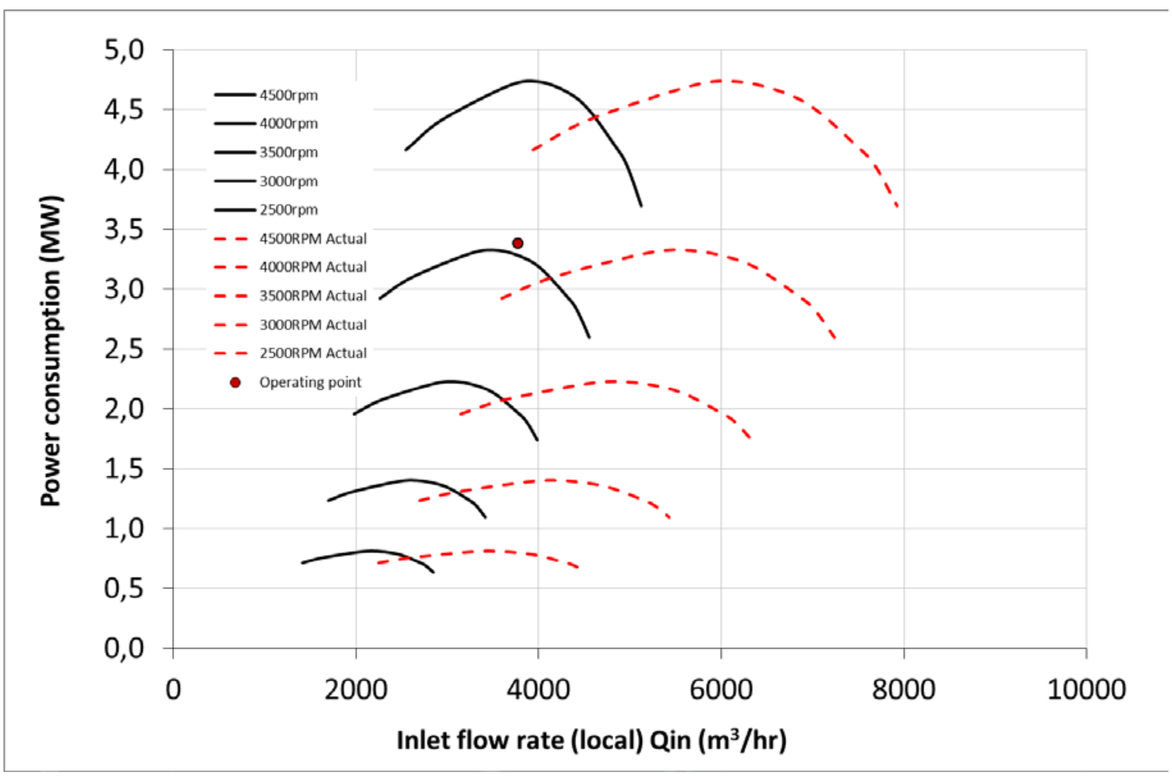

Figure 48. Compressor map, power, year 2022

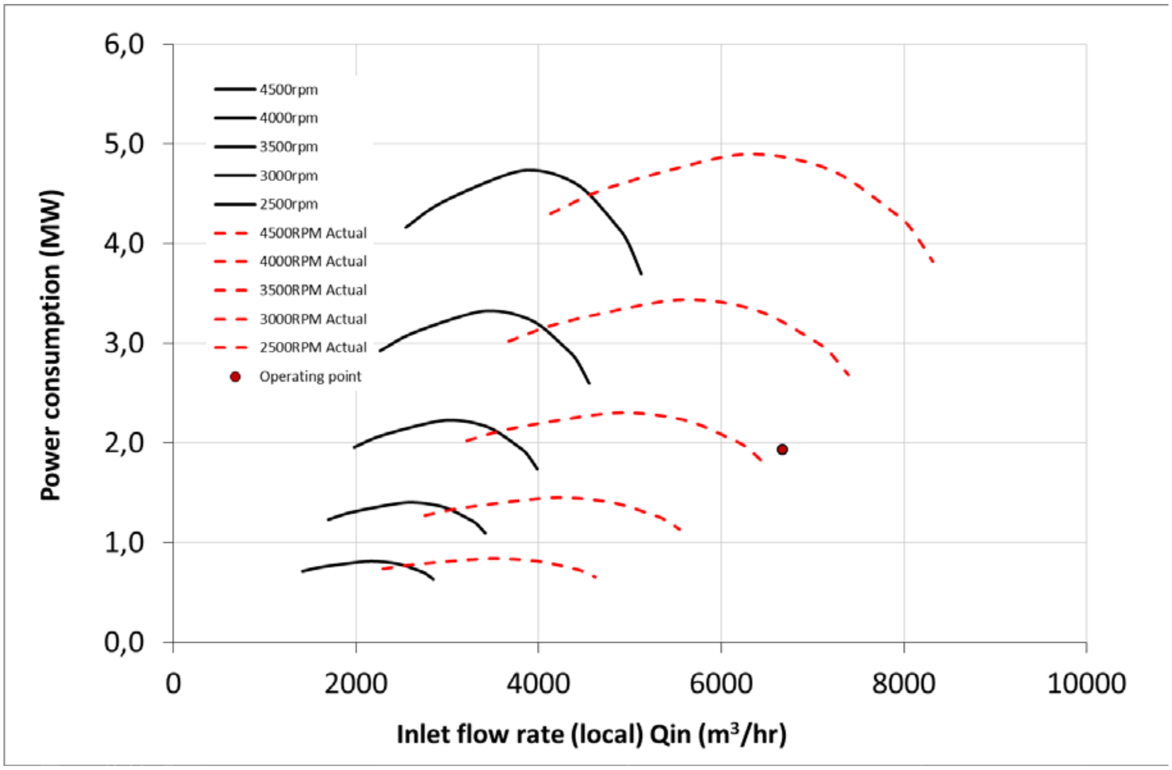

Figure 49. Compressor map, power, year 2023

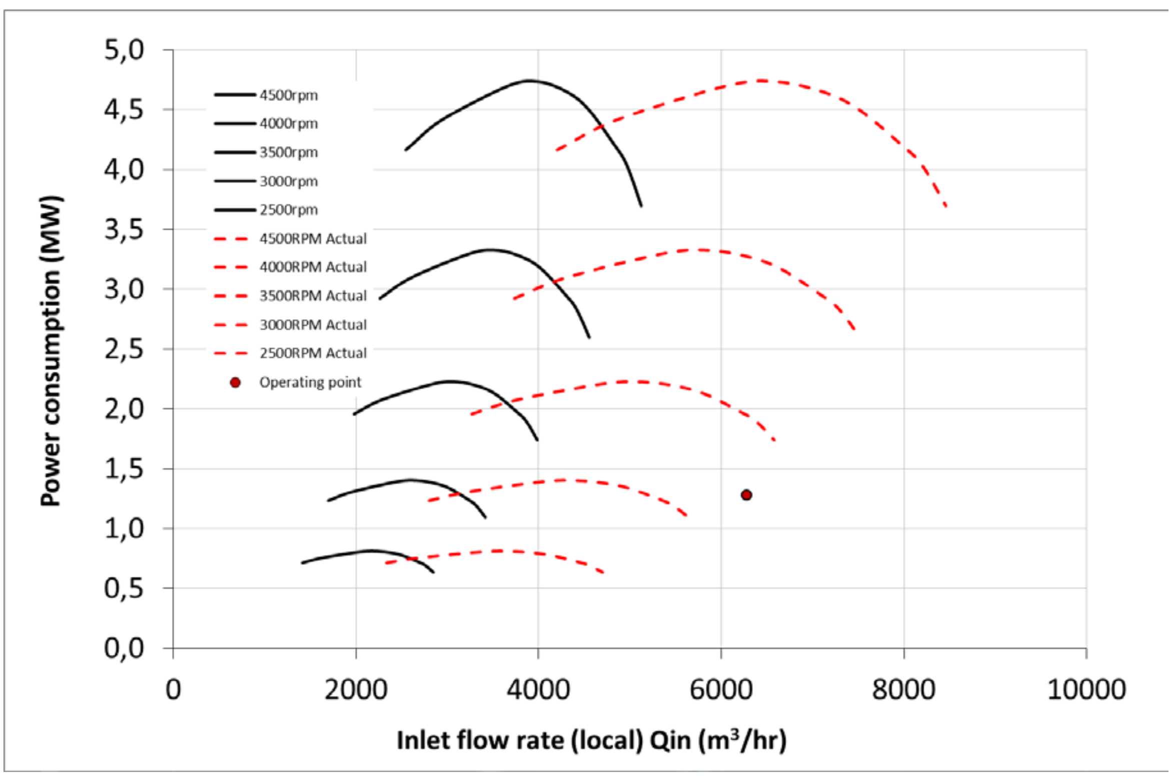

Figure 50. Compressor map, power, year 2024

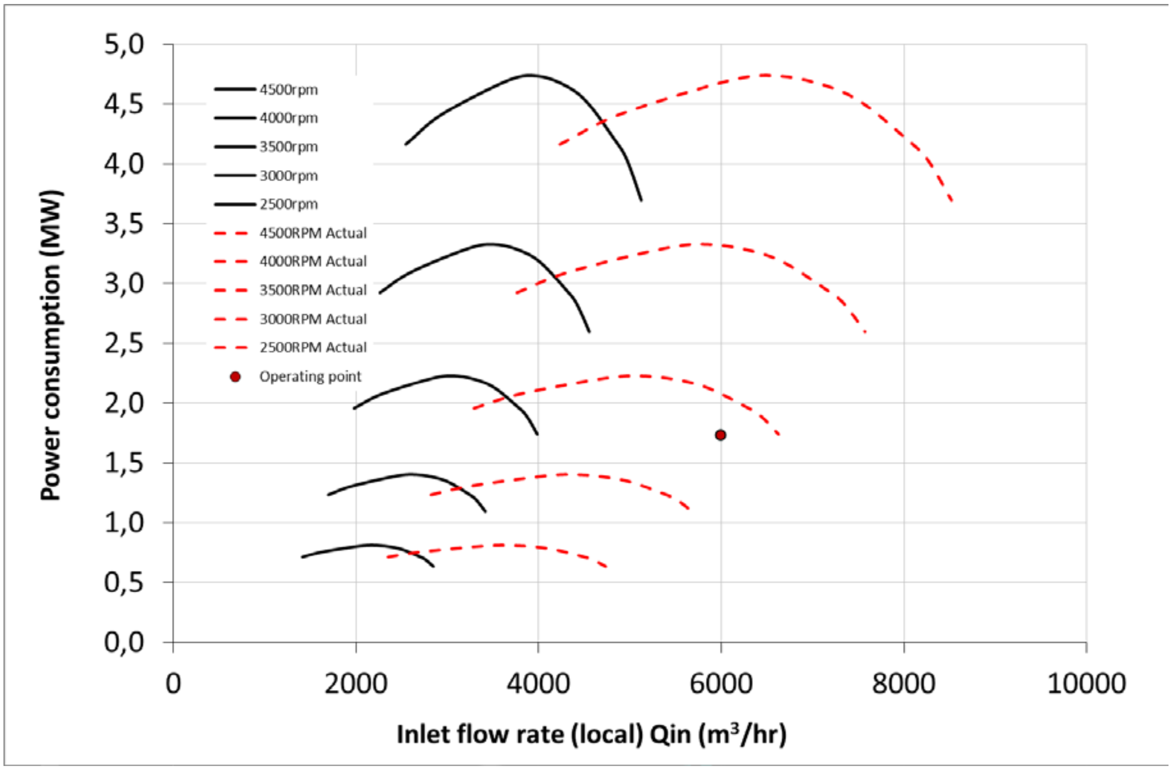

Figure 51. Compressor map, power, year 2025

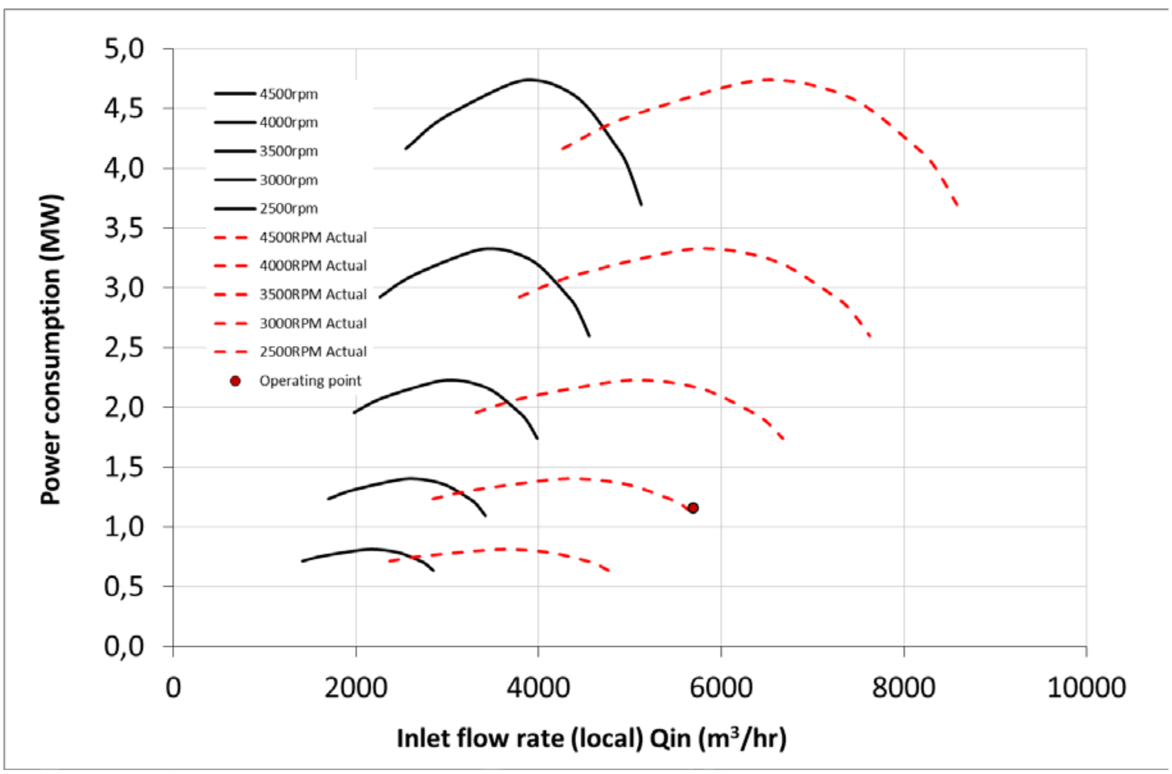

Figure 52. Compressor map, power, year 2026

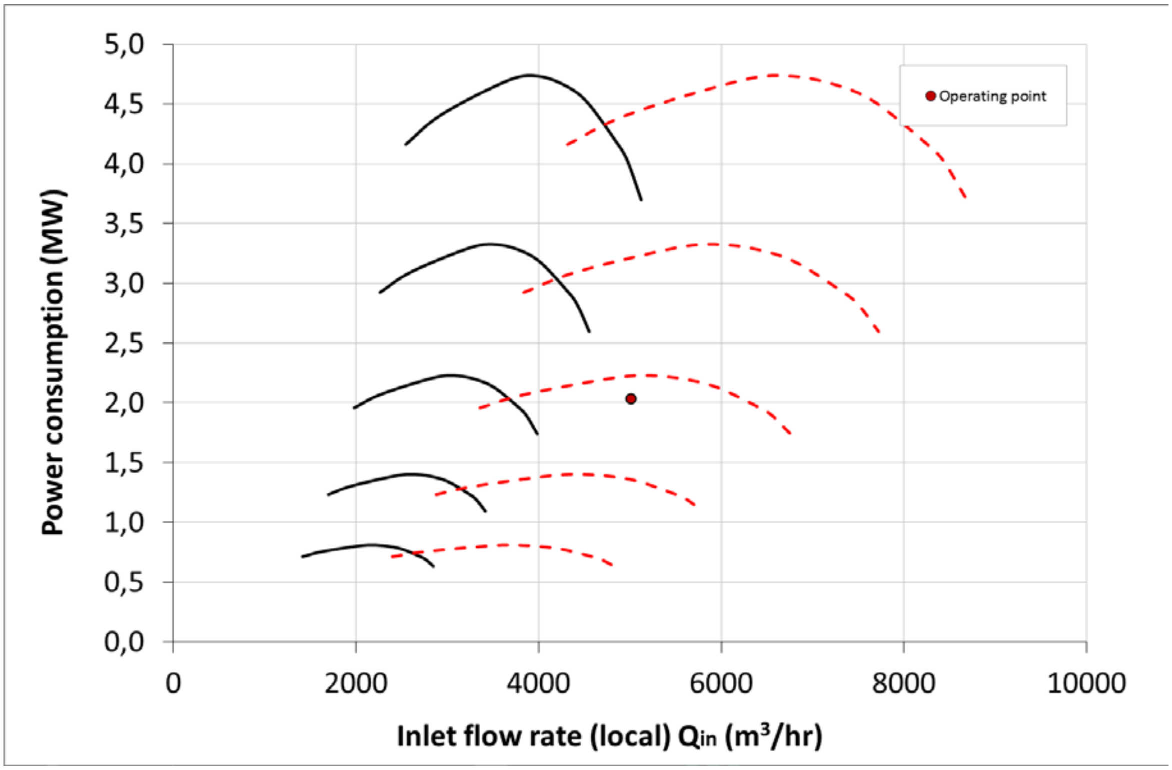

Figure 53. Compressor map, power, year 2027

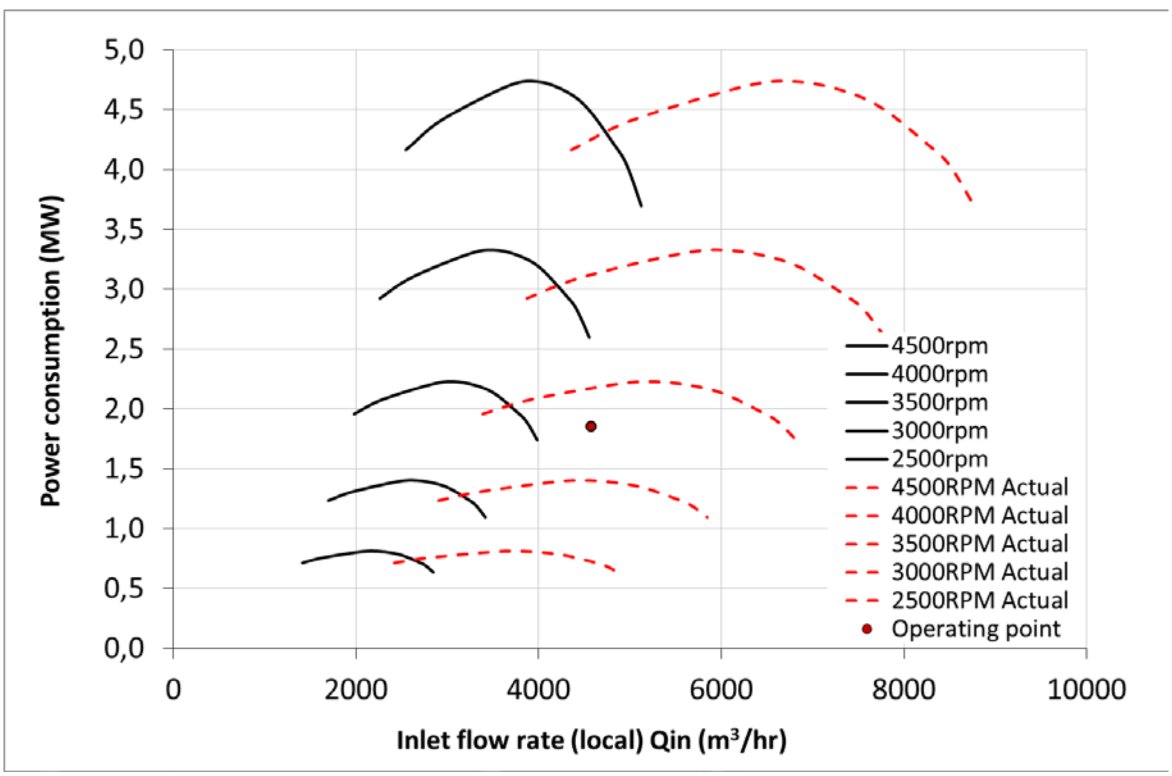

Figure 54. Compressor map, power, year 2028

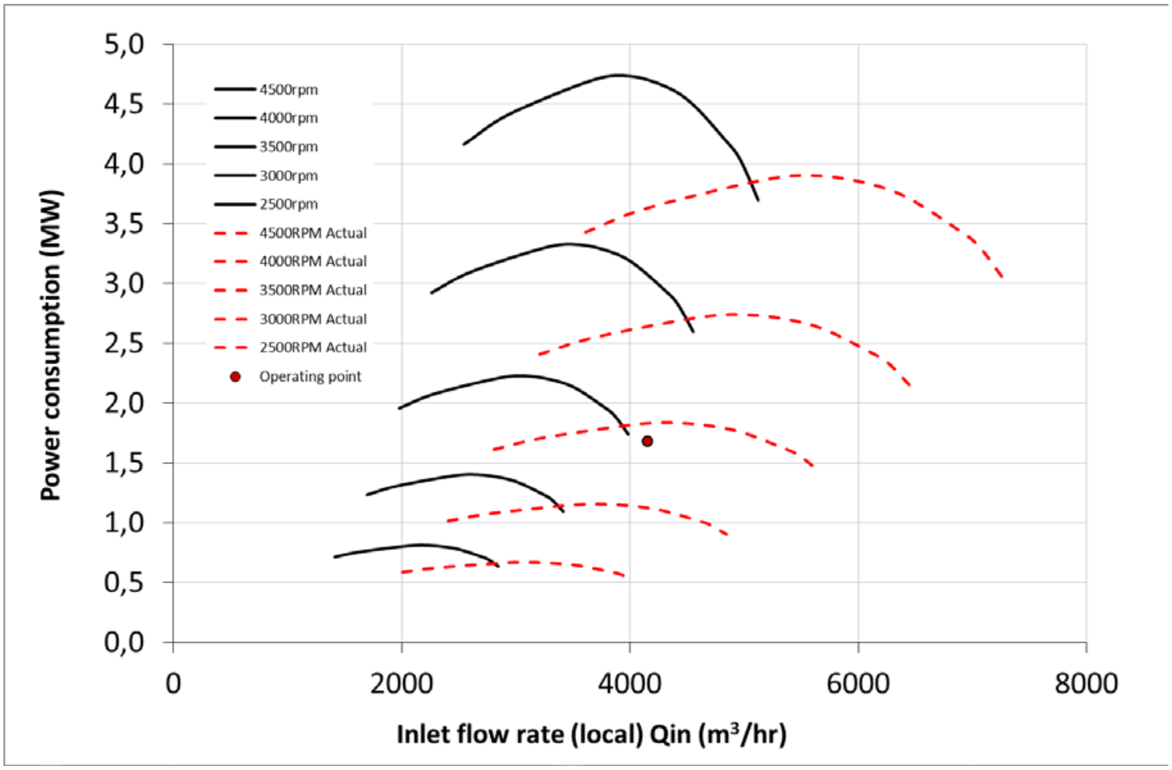

Figure 55. Compressor map, power, year 2029

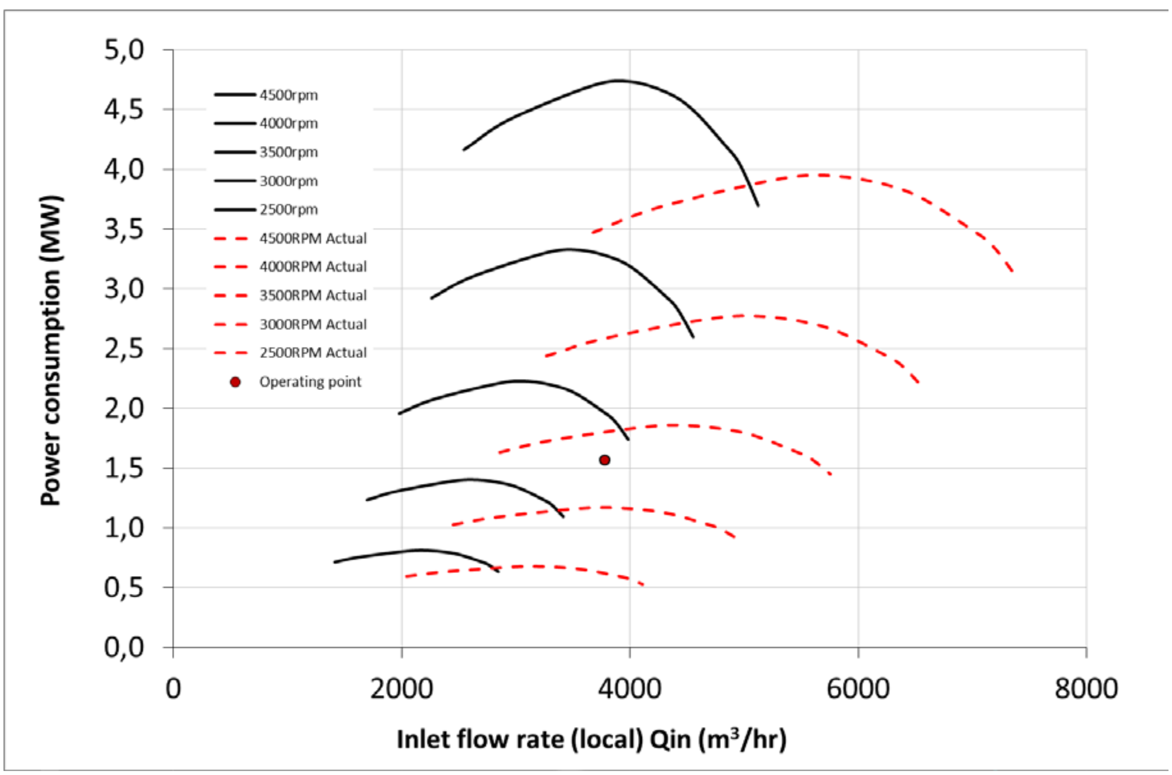

Figure 56. Compressor map, power, year 2030

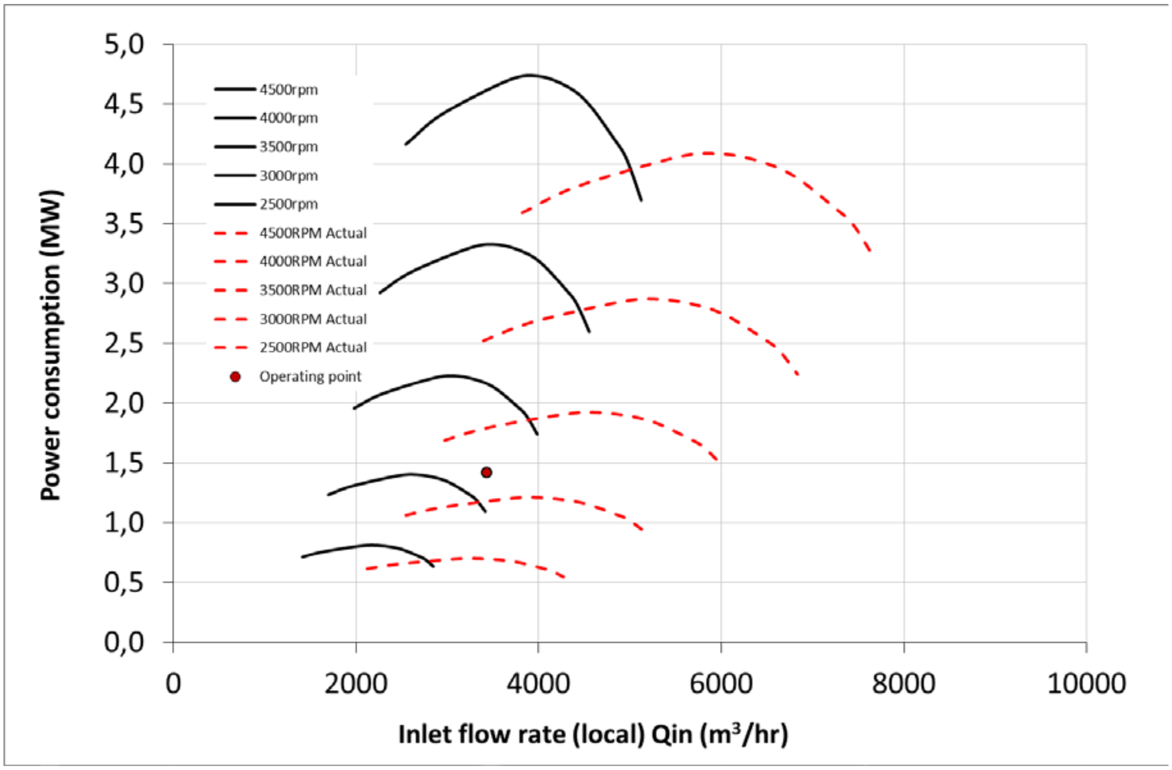

Figure 57. Compressor map, power, year 2031

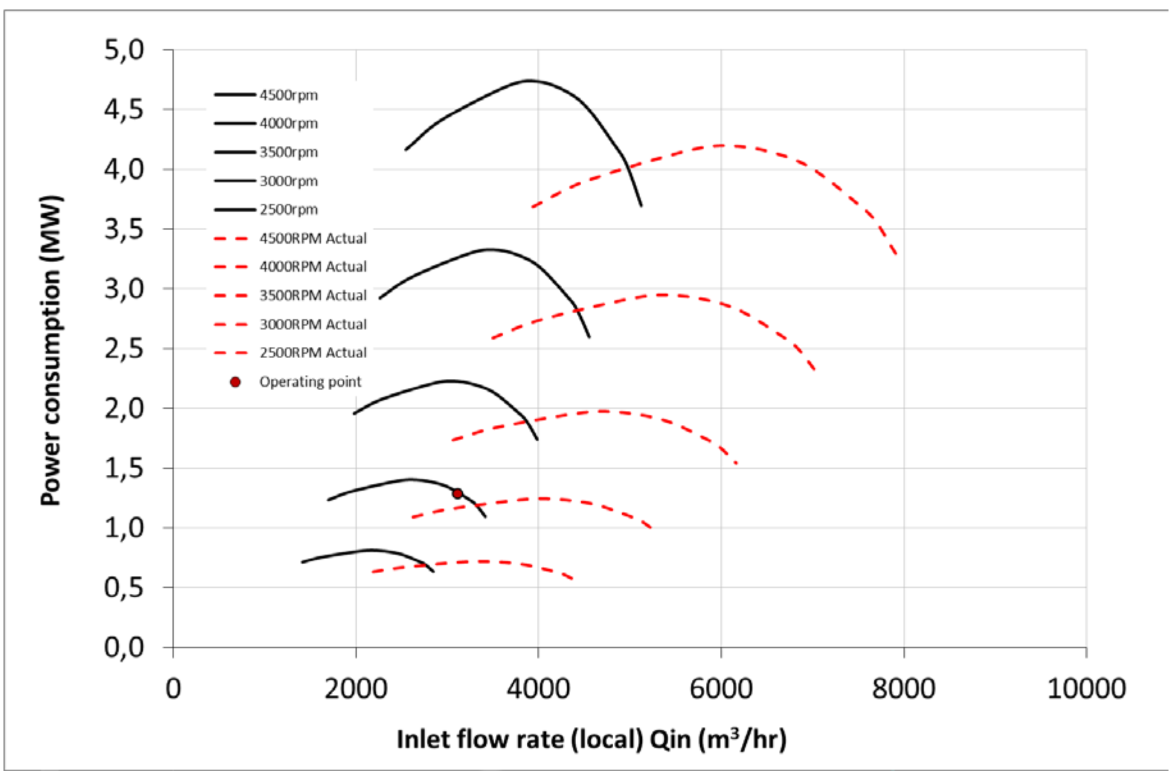

Figure 58. Compressor map, power, year 2032

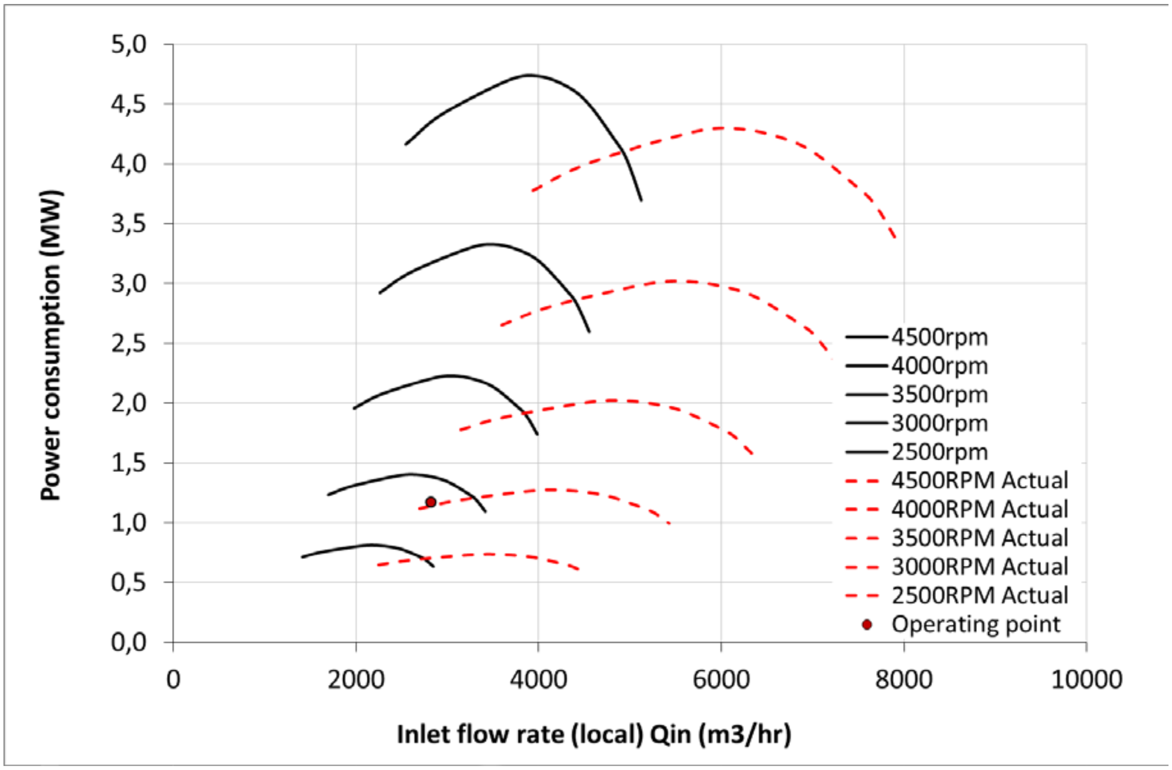

Figure 59. Compressor map, power, year 2033